

RNase P cleavage of pseudoknot substrates reveals differences in active site architecture that depend on residue N-1 in the 5' leader

David M. Kosek, J. Luis Leal, Ema Kikovska-Stojanovska, Guanzhong Mao, Shiying Wu, Samuel C. Flores & Leif A. Kirsebom

To cite this article: David M. Kosek, J. Luis Leal, Ema Kikovska-Stojanovska, Guanzhong Mao, Shiying Wu, Samuel C. Flores & Leif A. Kirsebom (2025) RNase P cleavage of pseudoknot substrates reveals differences in active site architecture that depend on residue N-1 in the 5' leader, RNA Biology, 22:1, 1-19, DOI: [10.1080/15476286.2024.2427906](https://doi.org/10.1080/15476286.2024.2427906)

To link to this article: <https://doi.org/10.1080/15476286.2024.2427906>



© 2025 The Author(s). Published by Informa UK Limited, trading as Taylor & Francis Group.



[View supplementary material](#)



Published online: 20 Jan 2025.



[Submit your article to this journal](#)



Article views: 283



[View related articles](#)



[View Crossmark data](#)

RESEARCH PAPER



RNase P cleavage of pseudoknot substrates reveals differences in active site architecture that depend on residue N-1 in the 5' leader

David M. Kosek^{a,b}, J. Luis Leal^{a,c}, Ema Kikovska-Stojanovska^{a,d}, Guanzhong Mao^a, Shiyong Wu^{a,e}, Samuel C. Flores^{a,f,g}, and Leif A. Kirsebom^a

^aDepartment of Cell and Molecular Biology, Biomedical Centre, Uppsala University, Uppsala, Sweden; ^bDepartment of Medical Biochemistry and Microbiology, Biomedical Centre, Uppsala University, Uppsala, Sweden; ^cDepartment of Ecology and Genetics, Evolutionary Biology Center EBC, Uppsala University, Uppsala, Sweden; ^dMerck Healthcare KGaA, Global Regulatory CMC & Devices, Darmstadt, Germany; ^eBio-Works AB, Uppsala, Sweden; ^fDepartment of Animal Biosciences, Swedish University of Agricultural Sciences, Uppsala, Sweden; ^gDepartment of Biochemistry and Biophysics, Stockholm University, Solna, Sweden

ABSTRACT

We show that a small biotin-binding RNA aptamer that folds into a pseudoknot structure acts as a substrate for bacterial RNase P RNA (RPR) with and without the RNase P C5 protein. Cleavage in the single-stranded region in loop 1 was shown to depend on the presence of a RCCA-motif at the 3' end of the substrate. The nucleobase and the 2'hydroxyl at the position immediately 5' of the cleavage site contribute to both cleavage efficiency and site selection, where C at this position induces significant cleavage at an alternative site, one base upstream of the main cleavage site. The frequencies of cleavage at these two sites and Mg²⁺ binding change upon altering the structural topology in the vicinity of the cleavage site as well as by replacing Mg²⁺ with other divalent metal ions. Modelling studies of RPR in complex with the pseudoknot substrates suggest alternative structural topologies for cleavage at the main and the alternative site and a shift in positioning of Mg²⁺ that activates the H₂O nucleophile. Together, our data are consistent with a model where the organization of the active site structure and positioning of Mg²⁺ is influenced by the identities of residues at and in the vicinity of the site of cleavage.

ARTICLE HISTORY

Received 27 February 2023
Revised 31 October 2024
Accepted 4 November 2024

KEYWORDS

RNase P; ribozyme; divalent metal ions; model substrates; tRNA processing

Introduction

The endoribonuclease P, RNase P, generates tRNAs with a single phosphate at their 5' termini. RNase P is composed of one RNA (RNase P RNA or RPR) moiety, while the number of protein subunits varies depending on origin: one protein in bacteria (in *Escherichia coli* referred to as the C5 protein), four to five in Archaea and nine to ten in Eukarya [1]. Irrespective of origin, the catalytic activity resides in the RPR [2–5]; however, RNase P activity solely composed of protein(s) exist as well [6–10].

Apart from being involved in tRNA processing, RNase P also processes several other natural RNAs, including mRNAs and riboswitches, the precursors to 4.5S RNA and tmRNA, synthetic model hairpin substrates, phage RNAs and small single-stranded RNAs [11–25]. Moreover, in RNA plant viruses such as the tobacco mosaic virus (TMV) and tobacco yellow mosaic virus (TYMV), the RNA 3' termini fold into a tRNA-like structure that ends with CCA. Folding of these structures depends on formation of a pseudoknot and these tRNA-like structures also act as RNase P substrates [26–30]. Pseudoknot structural

elements are also present in mRNAs, where they can influence the reading frame during translation [31,32]. Whether pseudoknots are targeted by RNase P *in vivo* remains an open question (see discussion). However, we emphasize that understanding factors that influence the processing of various RNA substrates, including pre-tRNAs and model substrates such as pseudoknot structures, is important to dissect and conceive the molecular features that determine efficient and correct RNase P processing.

The residue positioned 5' of the scissile bond (referred to as N₋₁ in e.g. precursor-tRNA) plays an important role in the processing of various substrates by RNase P, see e.g. [23, 33–40]. This has also been discussed to be the case for pseudoknot structures [30]. The structures of different pseudoknots have been studied in detail both by X-ray crystallography and nuclear magnetic resonance spectroscopy, NMR [41–47; for a review see 48]. Of these, the biotin-binding RNA aptamer is a pseudoknot structure of the hairpin (H-) type, and the crystal structure was solved at 1.3 Å resolution [49]. The pseudoknot in the TYMV tRNA-like structure, which was recently solved at 2.0 Å resolution [47], is another H-type pseudoknot. Since

CONTACT Leif A. Kirsebom  Leif.Kirsebom@icm.uu.se  Department of Cell and Molecular Biology, Biomedical Centre, Uppsala University, Box 596, Husargatan 3, Uppsala SE-751 24, Sweden

 Supplemental data for this article can be accessed online at <https://doi.org/10.1080/15476286.2024.2427906>

© 2025 The Author(s). Published by Informa UK Limited, trading as Taylor & Francis Group.

This is an Open Access article distributed under the terms of the Creative Commons Attribution License (<http://creativecommons.org/licenses/by/4.0/>), which permits unrestricted use, distribution, and reproduction in any medium, provided the original work is properly cited. The terms on which this article has been published allow the posting of the Accepted Manuscript in a repository by the author(s) or with their consent.

the TYMV tRNA-like structure acts as a substrate for RNase P [28–30], these structures are suited as experimental models towards understanding factors and the structure–function relation in cleavage mediated by RNase P and its RNA component, RPR.

The crystal structure of bacterial RNase P in complex with tRNA is available and represents a post-cleavage structure [50], and recently the cryo-EM structure of bacterial RNase P in complex with pre-tRNA was reported [51]. Albeit our understanding of the interaction between the 5' leader of the substrate and RNase P is increasing, the interaction between the RPR and residue N₋₁ in different substrates is limited. This is in particular true for how non-conventional substrates interact with the RPR. Given that *E. coli* (*Eco*) RPR with and without the C5 protein cleaves RNA pseudoknot substrates [28–30] we were interested in understanding whether the biotin RNA aptamer, for which a high-resolution structure is available [49], can act as substrate for *Eco* RPR. If so, study cleavage as a function of the nucleobase identity immediately 5' of the cleavage site (N₋₁ in pre-tRNAs) and its influence on the Mg²⁺ requirement, and use this information and available structures in modelling studies to extract information about the architecture at and in the vicinity of the cleavage site.

Here, we provide data showing that the biotin RNA aptamer [49] tagged with a 3' GCCAC trailer is cleaved by both bacterial (with and without the C5 protein) and archaeal RPR. The cleavage efficiency was, however, substantially lower compared to cleavage of other substrates such as model hairpin substrates [23]. Moreover, the identity of the nucleobase 5' of the cleavage site ('N₋₁') influences cleavage differently with respect to both site selection and efficiency of cleavage compared to cleavage of model hairpin substrates. Changing base pairs in the substrate in the vicinity of the cleavage site as well as in the RPR influenced site selection and Mg²⁺ binding. The data, complemented with dynamical modelling using MacroMoleculeBuilder (MMB), provided a rationale to the observed variation in site selection in response to changing the 'N₋₁' identity and its influence on Mg²⁺ requirement. Together, our data are consistent with a model where the structural architecture of the active site depends on the positioning of substrate residues and Mg²⁺ at, and in the vicinity of, the cleavage site. Finally, we foresee that our findings will enhance our understanding of RNase P processing of RNA molecules that contain pseudoknot structures such as mRNA *in vivo*.

Materials and methods

Preparation of substrates, RPRs and C5 protein

Substrates were purchased from Dharmacon (USA) and IBA GmbH (Germany) and purified on a 15% (w/v) denaturing PAGE gel followed by Bio-Trap extraction overnight (Schleicher and Schuell, GmbH, Germany; Elutrap in USA and Canada) and phenol-chloroform extraction. The different substrates were 5' end-labelled with [γ -³²P]-ATP and gel-purified as previously described [22,23].

The *Eco* RPR, *HyoP* RPR and *Pfu* RPR were generated as run-off transcripts using T7 DNA-dependent RNA polymerase and PCR-amplified templates [23, 52–54].

The *E. coli* C5 protein derivative, His6-C5, was purified as described elsewhere [23,55].

Biotin affinity chromatography

In the biotin-binding assays, 0.5 μ g of RNA substrate in buffer D [50 mM Tris-HCl (pH 7.5), 100 mM NH₄Cl, 10 mM MgCl₂] was applied on biotin agarose columns [prepared by adding 20 μ L biotin agarose to Pierce Micro-Spin Columns (Thermo Fisher, number 89879) and packed in microcentrifuge at 100 \times g]. The column was washed with five column volumes of buffer D. Bound RNA was eluted with five column volumes of buffer D containing 5 mM biotin. Following ethanol precipitation and re-suspension in double distilled water, the eluted RNA was quantified by measuring the absorbance at 260 nm using a NanoDrop.

Assay conditions

RPR-mediated cleavage without the C5 protein was conducted at 37°C in buffer C [50 mM MES (final pH 6.1), 0.8 M NH₄OAc] with indicated Mg(OAc)₂ concentrations. The RPR was pre-incubated in buffer C and Mg(OAc)₂ for 10 min to allow for folding into the active conformation, after which prewarmed (37°C) substrate was added. All the experiments in the absence of C5 were conducted under single turn over conditions with ≤ 0.02 μ M substrate. For the concentrations of *Eco* RPR, see table and figure legends.

Reactions with His6-C5 protein were carried out in buffer A [50 mM Tris-HCl, pH 7.2 (final), 100 mM NH₄Cl] supplemented with 10 mM MgCl₂. *Eco* RPR was pre-incubated in buffer A at 37°C for 10 min. The purified His6-C5 was added, followed by the addition of prewarmed (37°C) substrate and incubation for 30 min at 37°C. The concentrations of *Eco* RPR and His6-C5 were 0.004 μ M and 0.21 μ M, respectively, and the concentration of substrate was ≤ 0.02 μ M.

All reactions were terminated by the addition of two volumes of stop solution (10 M urea, 100 mM EDTA). Products were separated on 25% (w/v) denaturing polyacrylamide/7 M urea gels.

Determination of kinetic constants under single turnover conditions

The kinetic constants k_{obs} and $k_{\text{obs}}/K^{\text{sto}}$ ($=k_{\text{cat}}/K_{\text{m}}$) were determined under saturating single turnover conditions in buffer C (pH 6.1) and 800 mM Mg(OAc)₂ as described elsewhere, see e.g. [22,25]. The final substrate concentration was ≤ 0.02 μ M, while the *Eco* RPR concentration varied between 0.4 and 26 μ M, depending on RPR-substrate combination. For calculations, the 5' cleavage fragments were used to measure product formation. Incubation times were adjusted to ensure that the velocity measurements were in the linear range ($\leq 40\%$ of the substrate consumed). The k_{obs} and $k_{\text{obs}}/K^{\text{sto}}$ constants were obtained by linear regression from Eadie-Hofstee plots.

The K^{sto} ($\approx K_d$ [23]) constants were calculated using k_{obs} and $k_{\text{obs}}/K^{\text{sto}}$ values.

Substrate digestion with nuclease P1

Nuclease P1 was purchased from Sigma Aldrich (USA) and prepared according to company instructions. The RNA substrate was denatured at 95°C for 5 min and then added to buffer P1 (40 mM NaOAc, pH 5.3, 0.5 mM ZnSO₄) pre-warmed to 70°C. This was immediately followed by the addition of one ng (corresponding to ≥ 0.0002 units) nuclease P1 (Sigma Aldrich), to a final reaction volume of 10 μ L and incubation at 70°C for 1 min. The reaction was terminated by the addition of double volume of stop solution (10 M urea, 100 mM EDTA).

Modelling

MacroMoleculeBuilder, MMB (v. 2.19), is a general-purpose, multiscale, internal-coordinate macromolecular modelling code used for RNA modelling [56–58]. MMB is not a Molecular Dynamics (MD) package. MD works in cartesian coordinates whereas MMB works in internal coordinates, which eases implementation of integrative multiresolution modelling. However, internal coordinates greatly reduce the degrees of freedom of the system. Moreover, MMB uses water droplets, which are known to cause surface tension artefacts, unlike the water boxes typically used in MD. In earlier work, we showed that MMB and MD simulations are complementary, as MMB can create models that are easily sent on to MD for confirmation. Similarly, MMB can suggest tightly focused hypotheses for, or rationalization of, experimental results [59–61; see also below].

We used MMB to model the pseudoknot substrate in complex with RPR under solvation conditions. We used the crystal structure of RNase P in complex with tRNA (PDB code 3Q1R, resolution 4.2 Å [50]), replacing the tRNA with the biotin RNA aptamer crystal structure (PDB code 1F27, resolution 1.3 Å [49]). The Mg²⁺ concentration was set to one metal ion per 3.5 nucleotides (see e.g. [39] and references therein). These Mg²⁺ ions were initially placed well outside the cleavage site to prevent any biased results. The reported ion positions are the result of MMB dynamics, *i.e.* Coulomb and other interactions between ions, water, and RNA residues. The RPR-substrate complex was modelled independently for each variant (30 runs per variant).

Results

Importance of the N₉₍₋₁₎ identity for *Eco* RPR cleavage of a pseudoknot with and without the C5 protein

To understand whether the *in vitro* selected biotin-binding RNA aptamer can be cleaved by RNase P we generated pPK, which has the same sequence as reported by Nix et al. [49] (Figure 1A–C). pPK binds biotin suggesting that it acquired the expected fold. The unrelated RNA, pMini3bpUG, also binds biotin but with lower affinities (Figure 2A).

To test whether the pPK RNA is cleaved by *Eco* RPR_{wt} in the absence of the C5 protein we decided to perform the experiments discussed below at 800 mM Mg²⁺ (or as indicated). As we previously argued, at this Mg²⁺ concentration, the likelihood to detect cleavage increases. In addition, this would allow us to make comparison with previous findings using pre-tRNA and model hairpin substrates such as pMini3bp (Figure 1E) [23,25]. We also emphasize that in this study we focus on the RPR alone reaction since the C5 protein interacts with N₋₄ – N₋₈ in the pre-tRNA 5' leader (the corresponding residues are part of helix 1 in the pPK substrates) but not with N₋₁ and N₋₂ [63], which correspond to N₉ and N₈ in the pPK RNA (Figure 1A).

When we exposed this RNA to *Eco* RPR_{wt}, no apparent 5' cleavage product could be detected (Figure 2B, lanes 1 and 2). This is not surprising since pPK lacks the 3' RCC-motif that plays an important role in RPR-mediated cleavage (the RCCA-RPR interaction, interacting residues underlined, see also Figure 1D [64–68]). Hence, we designed a variant carrying the 5'-GCCAC trailer at the 3' end and this RNA is referred to as pPKA₉G₃₃. The N₉ residue corresponds to N₋₁ in pre-tRNAs and other model substrates and the underlined G (G₃₃, see Figure 1A) corresponds to the discriminator base at position +73 in tRNA (see below; Figure 1A, D and E [69]). The pPKA₉G₃₃ binds biotin with similar affinity as the original RNA aptamer structure suggesting that the 5'-GCCAC trailer does not induce changes in the structure that affect the binding affinity for biotin (Figure 2A).

Eco RPR cleaved pPKA₉G₃₃ generating a 9-nt long 5' cleavage product in the presence of 800 mM Mg²⁺ [25] and it co-migrated with the 5' fragment generated by cleavage of the well-characterized pATSerUG model substrate (Figure 2B, lane 5). This suggested that the cleavage site was between residues A₉ and G₁₀ (see Figure 1A–C). The 5' fragment also co-migrated with a nuclease P1 cleavage product suggesting that cleavage generated products with 5'-phosphate and 3'-hydroxyl groups at their ends as expected for RPR-mediated cleavage (Supplemental Figure S1; see e.g. [2,19]). We conclude that pPKA₉G₃₃ acts as substrate for *Eco* RPR_{wt} and it is cleaved mainly between residue A₉ and G₁₀. For comparison of choice of cleavage site using these substrates we hereafter refer to cleavage between positions 9 and 10 as 'c0' or the 'canonical' cleavage site, while cleavage between N₈ (C₈) and N₉ is referred to as the 'm-1' site (see below and Figure 1A–C). We emphasize that c0 and m-1 correspond to the +1 and -1 cleavage sites assignments used in previous studies of pre-tRNAs and other model substrates (cf. Figure 1A and E) [25].

For site selection and cleavage efficiency, the identity of the N₋₁ residue (N₉ in pPK) plays an important role in RPR-mediated cleavage of pre-tRNA and other model substrates (Figure 1E [23,25,39]). We therefore generated variants in which A₉ was substituted with C₉, G₉ and U₉ and these are referred to as pPKC₉G₃₃, pPKG₉G₃₃ and pPKU₉G₃₃, respectively (Figure 1A). These variants bind biotin with similar affinity as pPKA₉G₃₃ suggesting that the N₉ identity does not affect biotin binding (Figure 2A). *Eco* RPR_{wt} cleaved these three RNAs at the c0 site but interestingly the C₉ variant was also cleaved at the m-1 site (*i.e.* between N₈ and N₉; see above), with almost equal frequency as observed for cleavage

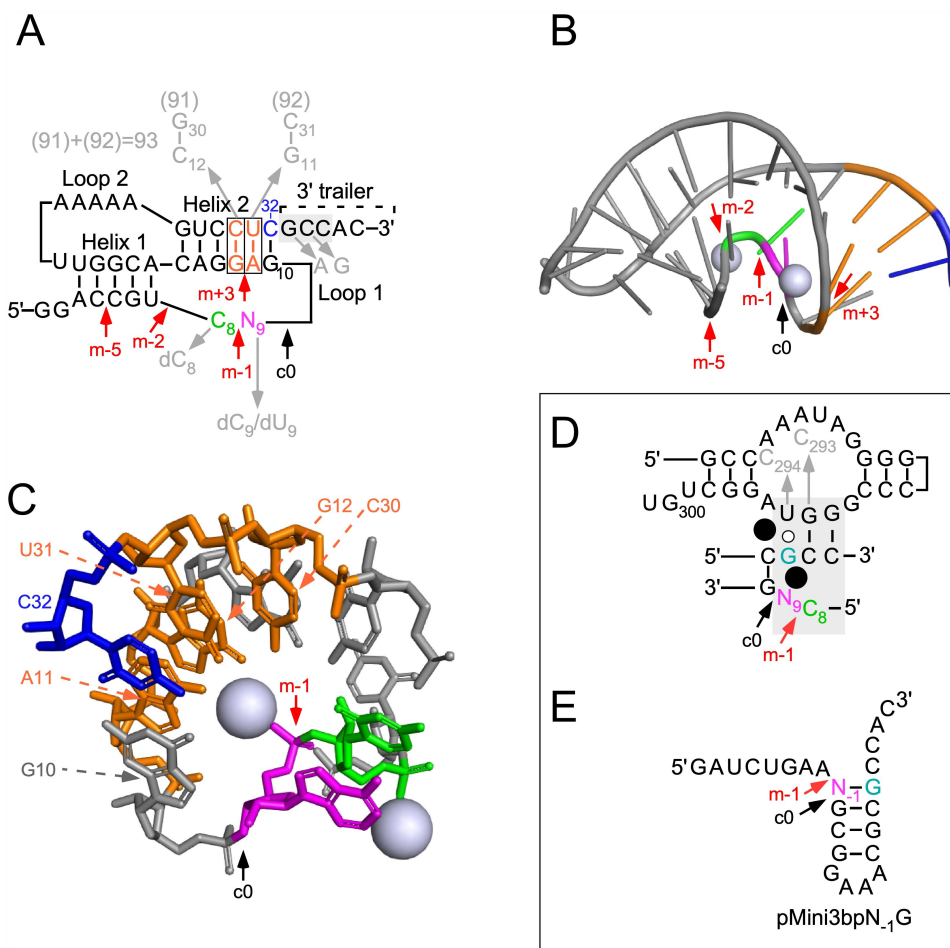


Figure 1. (A) Secondary structure of the pseudoknot (pPK) substrates used in the present study. Residue N₉, which is an A in the original pseudoknot [49], is marked in magenta and was changed to C, G and U as indicated in the main text. The grey arrows mark the replacement of the 2'-OH with 2'-H at C₉ (or U₉) and C₈ (highlighted in green), and replacement of nucleobases at indicated positions (marked in grey). The black arrow marks the c0 (canonical) cleavage site while the red arrows mark the alternative cleavage sites m-1, m-2 (see Figure 5), m+3 (cleavage at +3 was only detected using pPKU₉G₃₃, see main text) and m-5 (see Figure 5, cleavage with *HyoP* RPR). Residues in the grey box mark residues that interact with the RPR, see Figure 1D. The 5'-GCCAC-3' trailer was added as discussed in the main text. (B) The crystal structure of the pPK RNA biotin-binding aptamer at 1.3 Å, PDB 1F27 [49]. Residues discussed in the text are highlighted and coloured as in Figure 1A and 1C. The RPR cleavage sites are marked with arrows: c0 (canonical cleavage site) in black and the alternative cleavage sites m-1, m-2, m+3 and m-5 in red. The spheres represent Mg²⁺-ions. See also Figure 1A and 1C. (C) Part of the crystal structure of the original pPK RNA biotin-binding aptamer at 1.3 Å, PDB 1F27 [49]. Residues highlighted: A₉ (magenta), C₈ (green), the 3' terminal C₃₂ (blue), and A₁₁-U₃₁/G₁₂-C₃₀ (Orange). The spheres represent two Mg²⁺-ions and the arrows mark the cleavage sites c0 (black) and m-1 (red). (D) The RCCA-RNase P RNA interaction (interacting residues underlined and shown in the grey box) where the GCC sequence at the 3' termini pairs with G₂₉₂-G₂₉₃-U₂₉₄ in *Eco* RPR_{wt}. N₉, the residue immediately 5' of cleavage at c0 (black arrow) is highlighted in magenta and the alternative cleavage site m-1 is marked with a red arrow. The black spheres represent Mg²⁺ ions positioned in the vicinity of the cleavage site. The arrows marked in grey indicate the substitutions introduced in *Eco* RPR, for details see main text. The residue corresponding to the tRNA discriminator base is coloured in turquoise, see also the main text. (E) Secondary structure of pMini3bpN₁G. The black arrow marks the main cleavage site c0 while the red arrow marks the alternative site m-1. Note that c0 and m-1 correspond to cleavage at +1 and -1 as previously reported, for details see e.g. Wu et al. [23]. The residue corresponding to the tRNA discriminator base is coloured in turquoise, see also the main text.

at c0 (Figure 2B, lane 9; see also Supplemental Figure S1). As for pPKA₉G₃₃, these three N₉ variants generate 5' phosphate and 3' hydroxyl groups at their ends as a result of cleavage with *Eco* RPR_{wt} (Supplemental Figure S1).

The *Eco* RPR_{wt} alone reaction requires high Mg²⁺ while addition of the C5 protein lowers the Mg²⁺ requirement [2]. Typically, cleavage in the presence of C5 is conducted at 10 mM Mg²⁺ (see Materials and Methods). Addition of C5 resulted in similar cleavage patterns compared to what we observed in its absence at 800 mM Mg²⁺. Even the C₉ variant was cleaved both at the c0 and the m-1 sites albeit the frequency of cleavage at m-1 was slightly lower with C5 (Figure 2C). The A₉, G₉ and U₉ variants were predominantly cleaved at the c0 site with and without the C5 protein

(Figure 2B; data not shown for the A₉, G₉ and U₉ variants in the presence of C5). In this context, the rate of cleavage of pPKC₉G₃₃ at c0 (0.24 ± 0.028%/min) and m-1 (0.16 ± 0.022%/min) with C5 is similar as in the absence of C5 at 800 mM Mg²⁺, c0 (0.19 ± 0.0045%/min) and m-1 (0.17 ± 0.022%/min). Thus, addition of the C5 protein lowers the Mg²⁺ requirement but does not appear to influence the rate of cleavage relative to cleavage in the RPR alone reaction at 800 mM Mg²⁺.

Taken together, the biotin-binding RNA aptamer tagged with the 5'-GCCAC trailer at the 3' end acts as a substrate for *Eco* RPR with and without C5, and identity of the N₉ residue (the residue immediately 5' of the canonical cleavage, c0, site) plays a crucial role for site selection. In addition, despite that C₉ most likely does not pair (Figure 1A-C) with any residue

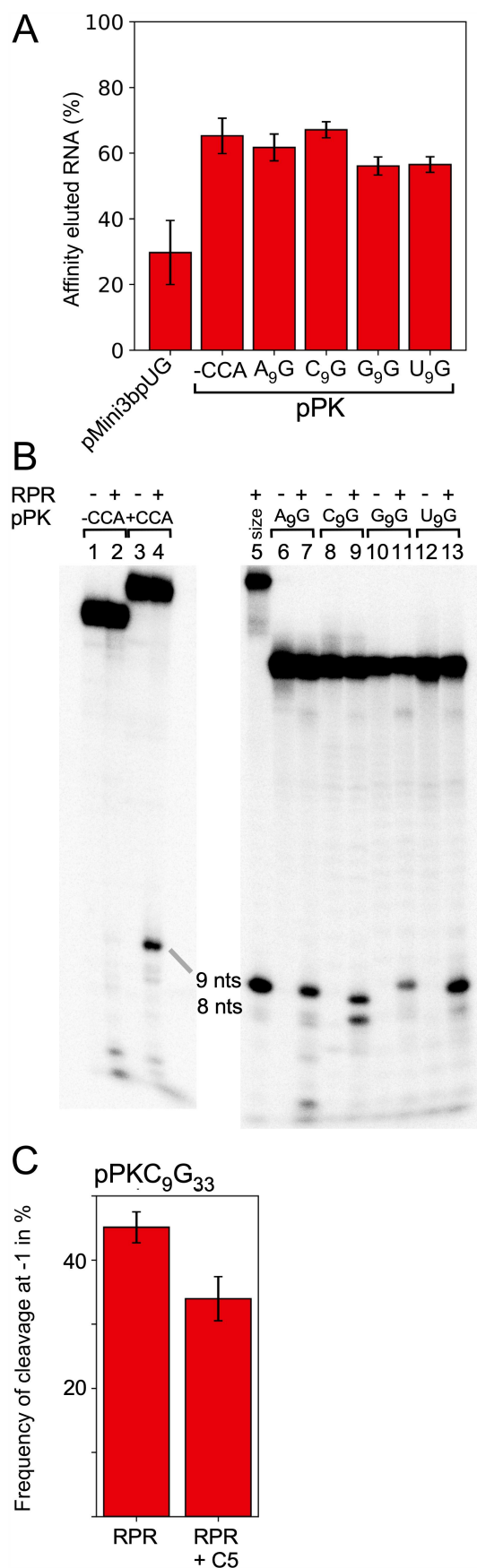


Figure 2. (A) Biotin binding. Amount of biotin-eluted pMini3bpUG and pPK RNA expressed as a percentage of total RNA applied to a biotin column (see Materials and Methods). The data represent mean \pm experimental errors calculated from at least three independent experiments. (B) Cleavage of pPK variants with *Eco*

in the substrate, it promotes cleavage at the alternative site m-1. This is in contrast to what we expected on the basis of previous studies using pre-tRNAs and model hairpin substrates, where the absence of pairing between residue N₋₁ and the discriminator base result in cleavage mainly at the c0 (+1) site [see e.g. Refs 25,39].

Cleavage as a function of divalent metal ions

Eco RPR_{wt} cleavage requires divalent metal ions, with a preference for Mg²⁺ considering both site selection and cleavage efficiency [70]. Hence, we first wanted to define the optimal Mg²⁺ concentration for cleavage of the pPKN₉G₃₃ variants. Determination of the cleavage rates as a function of increasing Mg²⁺ under single turnover conditions revealed that optimal rates were achieved at roughly 800 mM for the N₉ variants with the exception of pPKC₉G₃₃. For this variant ≥ 1000 mM was needed (saturation was not reached) irrespective of cleavage site, c0 or m-1 (Figure 3A). Following up on this observation, we analysed cleavage in the presence of combinations of divalent metal ions. We focused on Mg²⁺/Sr²⁺, Mg²⁺/Mn²⁺ and Mn²⁺/Sr²⁺ since for model hairpin substrates addition of Mn²⁺ promotes *Eco* RPR_{wt}-mediated cleavage at -1 (corresponds to m-1 in the pPKN₉G₃₃ substrates), while Sr²⁺ suppresses cleavage at this site [70,71]. In keeping with the influence of Mn²⁺ and Sr²⁺ on site selection, the C₉ substrate was cleaved preferentially at m-1 when we added Mn²⁺ while addition of Sr²⁺ reduced cleavage at m-1 (Figure 3B; note that in these experiments the final Me²⁺ concentration was 400 mM, see Materials and methods). For the A₉ variant, we detected increased frequency of cleavage at m-1 only in the presence of Mn²⁺ and Sr²⁺ while for the other Me²⁺ combinations (as indicated in Figure 3B), and the G₉ and U₉ variants (data not shown), cleavage was detected only at c0. We were unable to detect any cleavage in the presence of only Mn²⁺ or Sr²⁺ (not shown).

Together these data are consistent with a model where the N₉ identity influences positioning of divalent metal ion(s) at and in the vicinity of the cleavage sites (see Discussion).

The N₉ identity affects the kinetic constant k_{obs} and U₉ is preferred

Next, we determined the kinetic constants, k_{obs} and k_{obs}/K^{sto} , under single turnover conditions at saturating Mg²⁺ concentration (800 mM, non-saturating for pPKC₉G₃₃, see above and Figure 3A). The data revealed that k_{obs} for cleavage of pPKU₉G₃₃ at the c0 site was roughly six- to ten-fold higher compared to the other N₉ variants (Table 1). Calculating K^{sto} ($\approx K_d$; see [23]) suggested that *Eco* RPR_{wt} binds these pseudoknot substrates with similar affinities within a factor of two and irrespective of cleavage at c0 or at m-1 (see pPKC₉G₃₃; Table 1). Substituting G at position 33 in pPKU₉G₃₃ (Figure 1A; G₃₃ underlined in the GCCAC 3' trailer, see also above) with A generated pPKU₉A₃₃. This change resulted in a modest improvement in binding and k_{obs} (cf. pPKU₉G₃₃ vs. pPKU₉A₃₃; Table 1). In conclusion, our data suggest that the identity of N₉ primarily affects k_{obs} (with U at the N₉ position

being most favourable) while they bind to *Eco* RPR_{wt} with similar affinities (see also the Discussion).

Factors influencing site selection in cleavage of pPK substrates

The pPKA₉G₃₃ RNA lacking the 5'-GCCAC trailer (pPK) was not cleaved by *Eco* RPR_{wt} (see above). We therefore wanted to investigate the impact of the RCCA-RPR interaction (see above; interacting residues underlined) to get insight into how its structural topology affects cleavage of these pseudoknot substrates. We argued that, in accordance with our previous data, interference with this interaction would affect site selection, for a review see [72]. Hence, we substituted the C corresponding to 'C₇₄' in tRNA with G in pPKC₉G₃₃ (the 5'-GCCAC trailer changed to 5'-GGCAC; Figure 1A). This variant, pPKC₉G₃₃(G₃₄), was not cleaved by *Eco* RPR_{wt} while *Eco* RPR_{C293} (an RPR variant that restores pairing with G₇₄ in cleavage of pre-tRNA, see [64]) and Figure 1D cleaved this variant mainly at c0 and with significantly higher frequency than *Eco* RPR_{wt} cleaved pPKC₉G₃₃ at c0 (Figure 4A, cf. lanes 2 and 6). By contrast, *Eco* RPR_{C293} (which cannot pair with C₃₄ in pPKC₉G₃₃) cleaved pPKC₉G₃₃ almost exclusively at m-1 (see lane 3). We also analysed cleavage using *Eco* RPR_{C294} in which U₂₉₄, that pairs with the discriminator base N₇₃ in pre-tRNA (see Figure 1D; N₇₃ corresponds to N₃₃, see above), was replaced with C (see Figure 1A). Compared to *Eco* RPR_{wt}, *Eco* RPR_{C294} cleaved pPKC₉G₃₃ with reduced frequency at the m-1 site, while the other N₉ variants were cleaved at c0 (Figure 4B, and data not shown). Together, these findings emphasize the importance of formation and structural topology of the RCCA-RPR interaction for cleavage of pPKC₉G₃₃.

The N₋₁ 2'-OH (N₉ in pPKN₉G₃₃) in pre-tRNA and other substrates plays a crucial role in the RPR alone reaction with respect to site selection and cleavage efficiency, see e.g. [13,25,33–38,73–75]. Consistent with these previous findings, a 2'-H modification at C₉ in pPKC₉G₃₃ restricted cleavage to m-1, while a 2'H at C₈ directed cleavage predominately to the c0 site (Figure 4A, cf. lanes 8, 10 and 12). Introducing a 2'-H at position 9 in the U₉ variant also reduced cleavage at c0 but in contrast to pPKdC₉G₃₃, the dU₉ variant was cleaved at a new site, m+3 (between residues A₁₁ and G₁₂ in helix 2; Figures 1A and 4A, cf. lanes 14 and 16), but not at m-1. Hence, site selection depends on both N₉ identity and the 2'-OH at the position 5' of the cleavage site.

Next, we asked whether structural changes at other positions in pPKC₉G₃₃ affect site selection. We argued that substitution of chemical groups of bases in the vicinity of the cleavage site would influence the charge distribution and thereby affect the positioning of Mg²⁺ near the site of cleavage

(Figure 1A–C; coloured in orange). Thus, we designed and generated three pPKC₉G₃₃ variants where the orientations and identity of specific base pairs were changed (Figure 1A): pPKC₉G₃₃91 (G₁₂/C₃₀ changed to C₁₂/G₃₀), pPKC₉G₃₃92 (A₁₁/U₃₁ changed to G₁₁/C₃₁) and pPKC₉G₃₃93 (G₁₂/C₃₀ changed to C₁₂/G₃₀ and A₁₁/U₃₁ changed to G₁₁/C₃₁). *Eco* RPR_{wt} cleaved these three variants with reduced frequency at m-1 compared to pPKC₉G₃₃ [cf. Figure 3A (C₉G₃₃) vs. 3C (variants 91, 92 and 93); the frequency of cleavage at m-1 for pPKC₉G₃₃ was 46% while for pPKC₉G₃₃91, pPKC₉G₃₃92 and pPKC₉G₃₃93 the frequencies were 31%, 38% and 34%, respectively]. Also, relative to pPKC₉G₃₃ a lower Mg²⁺ concentration was required for optimal cleavage irrespective of variant and cleavage site (cf. Figure 3A and C). Determination of k_{obs} and k_{obs}/K^{sto} for pPKC₉G₃₃93 (Table 1) revealed that the reduced cleavage at m-1 is due to a ≈ two-fold increase in k_{obs} for cleavage at c0 while only a minor increase (≈30%) in k_{obs} at m-1 was detected relative to cleavage of pPKC₉G₃₃ at these sites. Noteworthy, we did not detect any substantial difference in binding, cf. K^{sto} (≈K_d) values for pPKC₉G₃₃ and pPKC₉G₃₃93 (Table 1). Relative to the other factors discussed above, the results of changing the orientations and identity of these base pairs on cleavage were modest. Nevertheless, we interpret these data to suggest that changing the structural topology facing the cleavage site influence site selection and Mg²⁺ requirement/binding.

Cleavage of the pPKN₉G₃₃ variants with bacterial type B and archaeal RPR

On the basis of secondary structure bacterial RPR can be divided into type A (Ancestral) and type B (Bacillus) where *Eco* RPR represents type A. *HyoP* RPR from *Mycoplasma hyopneumoniae* is a type B representative, while the archaeal *Pyrococcus furiosus* (*Pfu*) RPR belongs to type A. Both these RPRs are catalytically active in the absence of RNase P proteins [4,52,53]. Hence, we asked whether these two RPRs can cleave the pseudoknot pPKN₉G₃₃ variants. The results in Figure 5 show that *HyoP* RPR cleaved the C₉ variant at m-1, while the U₉ variant was cleaved at c0. For the A₉ and G₉ variants, we detected very weak (if any, in particular for the A₉ variant) cleavage mainly at m-2 between U₇ and C₈. Noteworthy, all the N₉ variants were also cleaved at m-5 between C₄ and C₅ (Figure 1A, B). For *Pfu* RPR, we detected cleavage for all four N₉ variants and the C₉ and G₉ variants were cleaved at both c0 and m-1. The G₉ variant was also cleaved at m-2, i.e. between U₇ and C₈ (Figure 1A).

These data show that these pseudoknot RNAs also act as substrates for other RPRs but site selection varies and depends on the RPR. Conceivably this is related to structural

RPR_{wt} in buffer C at 800 mM Mg(OAc)₂ as indicated. The concentration of substrate was ≤0.02 μM while the *Eco* RPR_{wt} concentration was 6.4 μM (pPK) and 0.8 μM for the pATSerUG control (ctrl) in lane 5. Lane 1, pPK lacking the 5'-GCCAC 3' trailer without RPR, incubation for 360 min; lane 2, pPK lacking the 5'-GCCAC 3' trailer with RPR, incubation for 360 min; lane 3, pPK (pPKA₉G₃₃) with the 5'-GCCAC 3' trailer without RPR, incubation for 90 min; lane 4, pPK (pPKA₉G₃₃) with the 5'-GCCAC 3' trailer with RPR, incubation for 90 min; lane 5, pATSerUG (5' leader size control) with RPR, incubation for 5 s; lane 6, pPKA₉G₃₃ without RPR, incubation for 90 min; lane 7, pPKA₉G₃₃ with RPR, incubation for 90 min; lane 8, pPKC₉G₃₃ without RPR, incubation for 60 min; lane 9, pPKC₉G₃₃ with RPR, incubation for 60 min; lane 10, pPKG₉G₃₃ without RPR, incubation for 90 min; lane 11, pPKG₉G₃₃ with RPR, incubation for 90 min; lane 12, pPKU₉G₃₃ without RPR, incubation for 60 min; lane 13, pPKU₉G₃₃ with RPR, incubation for 60 min. 9 and 8 nts mark the size of the 5' cleavage product and the upper band the uncleaved substrate. (C) Frequency of cleavage of pPKC₉G₃₃ at m-1 with *Eco* RPR_{wt} in the absence and presence of C5. The frequency of cleavage at m-1 was determined as previously described [23,25] and represents the mean ± experimental errors of at least three independent experiments.

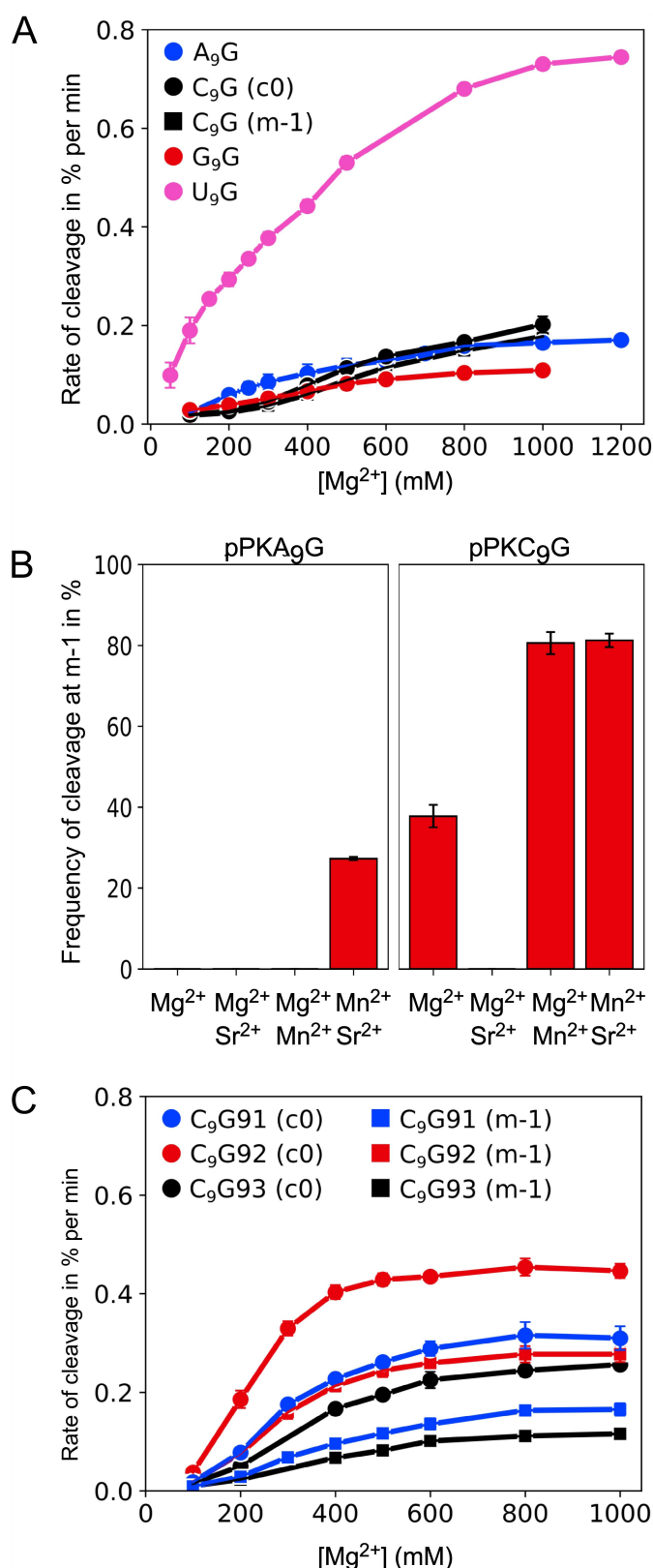


Figure 3. Cleavage of the pPKN₉G variants with *Eco* RPR_{wt} as a function of Mg²⁺ concentration or different Me²⁺ combinations. (A) Mg²⁺ profiles for pPKN₉G. The rate of cleavages as a function of Mg²⁺ concentration at c0 for pPKA₉G₃₃, pPKG₉G₃₃ and pPKU₉G₃₃ (marked as AG, GG and UG, respectively), and at c0 and m-1 for pPKC₉G₃₃ (marked as CG). The substrate concentration was ≤0.02 μM and the *Eco* RPR_{wt} concentration was 3.2 μM irrespective of substrate. The experiment was performed under single-turnover conditions at 37°C as described in Materials and Methods, and the cleavage rates (in % per min) represent the mean ± experimental errors of at least three independent experiments. (B) Frequency of cleavage of pPKA₉G₃₃ and pPKC₉G₃₃ at c0 and m-1 in

differences. Comparing the type A *Eco* RPR and type B *HyoP* RPR, e.g. for *Eco* RPR the substrate ‘3’-RCC-motif interacts with an internal loop (Figure 1D) while in the case of *HyoP* RPR this interaction involves a loop structure [65]. Albeit *Pfu* RPR belongs to type A RPR, there are structural differences compared to *Eco* RPR e.g. the P18 element is lacking in *Pfu* RPR (Figure 7). Whether this is the reason why the G₉ variant is cleaved by *Pfu* RPR at several sites (see Figure 5) requires further investigation. We also emphasize that we have reported differences in cleavage of other model substrates by *Eco* RPR vs. *Pfu* RPR [53,78].

Modelling the interaction between *Eco* RPR and pPK substrates

To understand the difference in cleavage site selection for pPKC₉G₃₃ relative to the other variants we modelled the interaction between RPR and the different pPKN₉G₃₃ derivatives. For this purpose, we used the *Thermotoga maritima* RNase P (type A RPR) structure in complex with tRNA^{Phe} [50], the structure of the biotin-binding RNA aptamer [49] and the macromolecular modelling code MMB [56,61] as outlined in Materials and Methods. Traditional Molecular Dynamics (MD) is the most widely used means of dynamical atomistic physics-based modelling of macromolecules. However, MD does not work as well for RNA as it does for proteins, regarding accuracy and runtime. If an initial 3D structure is not available, MD will struggle to fold the RNA and place ions correctly in a reasonable amount of time. MacroMoleculeBuilder (MMB) can quickly convert limited information about base-pairing into 3D structure [56,61]. It can also apply Coulomb and van der Waals forces [62] and place an explicit-water droplet surrounding a region of interest. Within such droplets ions can quickly travel to form electrostatically favourable interactions with both RNA and water. MMB can quickly yield insights that help explain biochemical phenomena [61].

Canonical and alternative cleavage events observed for the C₉ variant

Post-equilibration conformations for RNase P in complex with pPKC₉G₃₃ are shown in Figure 6. Conformations judged to induce cleavage at the c0 site (between C₉ and G₁₀; Figure 6A and B) require the presence of Mg²⁺ (marked in green), which activates H₂O for an inline nucleophilic attack (green dashed line) from the opposite side of the scissile phosphate relative to the C₉ 2’-OH (see e.g. Ref [39]). The distance between the Mg²⁺ and the scissile phosphate varied between 5.2 and 7.4 Å (with a mean value and standard variation equal to 6.2 ± 0.6 Å), a distance allowing space for the H₂O responsible for the nucleophilic attack [23,39,72,79,80]. Functional groups in the ligand sphere of this Mg²⁺ include the phosphate groups of A₁₁ (in pPKC₉G₃₃) and the O-4 of U₆₉ (*Eco* RPR numbering and corresponding to U₅₂ in the RNase P-tRNA structure [50]). Geometries compatible with an in-line canonical cleavage event (Figure 6A) were also associated with the presence of a binding configuration where an adjacent Mg²⁺ (marked in red) is surrounded by phosphate groups linked to G₁₀ in

Table 1. The kinetic constants k_{obs} and $k_{\text{obs}}/K^{\text{sto}}$ for cleavage of various pseudoknot substrates at 800 mM Mg^{2+} with $\text{Eco RPR}_{\text{wt}}$.

Substrate	Cleavage site	k_{obs} (min^{-1})	$k_{\text{obs}}/K^{\text{sto}}$ ($\text{min}^{-1}\mu\text{M}^{-1}$)	K^{sto} ($\approx K_d$)# (μM)
pPKA ₉ G ₃₃	c0	$(19 \pm 1) \times 10^{-4}$	$(70 \pm 12) \times 10^{-4}$	0.27
pPKG ₉ G ₃₃	c0	$(12 \pm 0.64) \times 10^{-4}$	$(25 \pm 8.4) \times 10^{-4}$	0.48
pPKU ₉ G ₃₃	c0	$(120 \pm 11) \times 10^{-4}$	$(490 \pm 140) \times 10^{-4}$	0.24
pPKU ₉ A ₃₃	c0	$(170 \pm 13) \times 10^{-4}$	$(1200 \pm 290) \times 10^{-4}$	0.14
pPKC ₉ G ₃₃	c0	$(21 \pm 0.8) \times 10^{-4}$	$(70 \pm 12) \times 10^{-4}$	0.30
	m-1	$(16 \pm 0.72) \times 10^{-4}$	$(74 \pm 3.9) \times 10^{-4}$	0.22
pPKC ₉ G ₃₃ 93	c0	$(47 \pm 1.3) \times 10^{-4}$	$(150 \pm 14) \times 10^{-4}$	0.31
	m-1	$(21 \pm 0.74) \times 10^{-4}$	$(80 \pm 10) \times 10^{-4}$	0.26

The experiments were performed under saturating single turnover conditions at 800 mM Mg^{2+} at pH 6.1 as described in Materials and Methods. The final concentration of substrate was $\leq 0.02 \mu\text{M}$. The concentration of the different *Eco RPR* variants was varied between 0 and 26 μM and the concentration range varied dependent on *Eco RPR* variant and substrate. The data represent mean \pm experimental errors calculated from at least three independent experiments. #The K^{sto} values were calculated using k_{obs} and $k_{\text{obs}}/K^{\text{sto}}$ values.

pPKC₉G₃₃, and to three RPR residues A₆₇, A₃₅₁, and A₃₅₂ (Figure 6A; *Eco RPR* numbering Figure 7; A₆₇, A₃₅₁ and A₃₅₂ correspond to A₅₀, A₃₁₃ and A₃₁₄ in the crystal structure of the RNase P-tRNA complex [50]; hereafter we follow *Eco RPR* numbering). Occasionally, G₆₈ was also observed to be present. A second metal-ion binding site was also observed (marked in blue in Figure 6A and B), albeit its nucleotide composition was less conserved, covering any of the combinations such as C₉-U₆₉, G₁₀-A₁₁-G₆₈, or C₉-G₁₀-A₁₁-G₆₈ (U₆₉ and G₆₈ correspond to residues in *Eco RPR*).

Presence of these two Mg^{2+} binding sites, however, did not suffice to guarantee a canonical cleavage conformation. The precise orientation of the G₁₀ phosphate group depends on the conformation of the pPKC₉G₃₃ backbone in this highly populated region of the complex (Figure 6B). Backbone torsion angles are in turn affected by small variations in the position of the surrounding RPR residues, which influence the orientation of C₈ and C₉ in pPKC₉G₃₃. As a consequence, for several of the dynamical modelling runs the resulting equilibrium conformation did not conform to a geometry compatible with positioning Mg^{2+} for an in-line attack (see above) and cleavage at the c0 site (*i.e.* the canonical site). Instead, in a subset of these runs the position of Mg^{2+} (marked in green) favoured an in-line attack and cleavage at the alternative site (m-1) between C₈ and C₉ (Figure 6C, see also Figure 1). Whenever an ion was observed in position to activate the water nucleophile for cleavage at m-1, phosphate groups linked to G₁₀, A₁₁ and the RPR residue U₆₉, referred to as the 'G₁₀-A₁₁-U₆₉' configuration, always surrounded the Mg^{2+} suggested to be involved in coordinating the H₂O nucleophile for an in-line nucleophilic attack. Our results suggest that this configuration is necessary for cleavage to occur at the alternative site m-1. Further substantiating the robustness of this model, for the set of runs involving pPKC₉G₃₃, a similar number of cleavage events were observed for the canonical and alternative configuration. These findings agree with the experimental data (see above, *e.g.* Figure 2B and Table 1).

The G₁₂/C₃₀ to C₁₂/G₃₀ switch in pPKC₉G₃₃ destabilizes the configuration at the alternative cleavage site

Introducing changes at positions distant to the cleavage sites in pPKC₉G₃₃ reduced the frequency of cleavage at m-1 (see above and *cf.* Figures. 1, 2C, 3A,C). Changing G₁₂/C₃₀ to C₁₂/G₃₀, as in pPKC₉G₃₃91, had minimal impact on the configuration around the canonical cleavage site c0 (Figure 8A). The number of runs yielding a conformation compatible with cleavage at the m-1 site (between C₈ and C₉; see Figure 1), however, decreased by 80%. This dramatic decrease was consistent with a similar change in the number of dynamical modelling runs resulting in the 'G₁₀-A₁₁-U₆₉' configuration discussed above. Moreover, this configuration was retained for the few events resulting in cleavage at the alternative site m-1 confirming that this configuration is necessary for cleavage at this site. Hence, the G₁₂/C₃₀ to C₁₂/G₃₀ change seems to disturb the positioning and binding patterns of Mg^{2+} located in the vicinity, creating a scenario where the 'G₁₀-A₁₁-U₆₉' configuration required for cleavage at the alternative site m-1 is energetically less favourable. This provides a rationale for the change in site selection, cleavage efficiency and difference in Mg^{2+} requirement observed experimentally comparing pPKC₉G₃₃ and the pPKC₉G₃₃ '91-93' variants (see above).

For the A₉, G₉ and U₉ variants the 'G₁₀-A₁₁-U₆₉' configuration at the m-1 site is absent

Dynamical modelling runs for the A₉, G₉ and U₉ variants suggested conformations compatible only with cleavage at the c0 site (Figure 8B-D). Depending on the N₉ identity, substrate residues adjust their positions vis-à-vis the RPR differently and the RPR residues involved are different from those observed with the C₉ variant (Figure 6A, B). However, this does not seem to affect cleavage at the c0 site to any significant extent since these conformations do not favour the 'G₁₀-A₁₁-U₆₉' configuration associated with cleavage at the

the presence of Mg^{2+} (400 mM), Mg^{2+} (150 mM) and Sr^{2+} (250 mM), Mg^{2+} (250 mM) and Mn^{2+} (150 mM), and Mn^{2+} (150 mM) and Sr^{2+} (250 mM). The concentration of substrate was $\leq 0.02 \mu\text{M}$ while the *Eco RPR*_{wt} concentration was 6.4 μM . The experiments were performed under single-turnover conditions in buffer C (total Me^{2+} concentration 400 mM) at 37°C as outlined in Materials and Methods and time of incubation was 300 min. The frequencies at m-1 represent the mean \pm experimental errors of at least three independent experiments, see also Figure legend 2C. We emphasize, for those combinations where we did not detect cleavage at m-1 are shown as zero frequency of cleavage at m-1. (C) Rates of cleavage for pPKC₉G₃₃91 (CG91) at c0 and m-1, pPKC₉G₃₃92 (CG92) at c0 and m-1, and pPKC₉G₃₃93 (CG93) at c0 and m-1 as a function of Mg^{2+} concentration. The experiment was performed under single-turnover conditions at 37°C as described in Materials and Methods, and the cleavage rates (in % per min) represent the mean \pm experimental errors of at least three independent experiments (see also above under A).

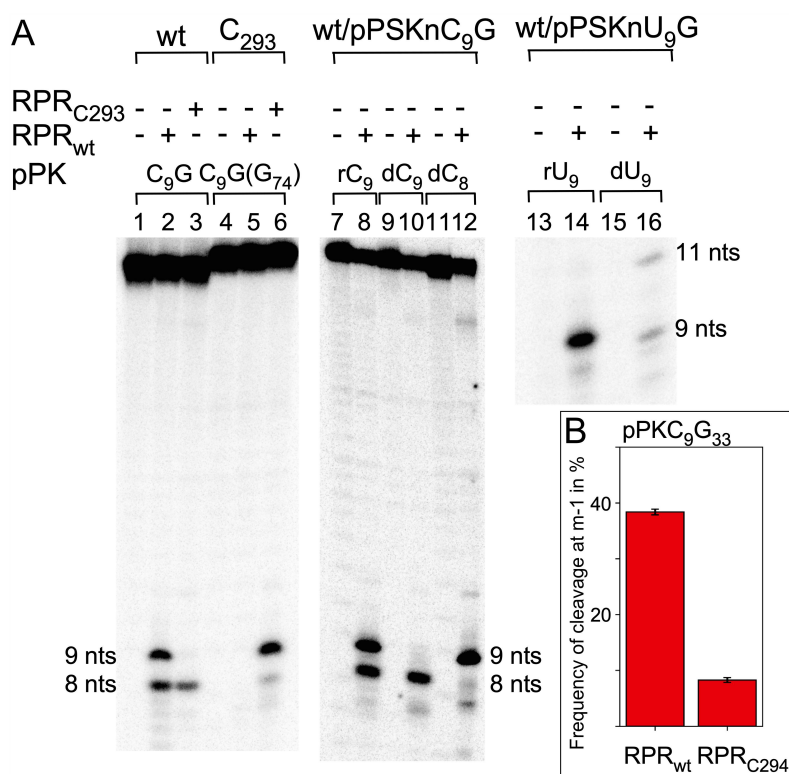


Figure 4. Cleavage of pPKC₉G₃₃ and pPKU₉G₃₃ variants with different *Eco* RPRs in buffer C at 800 mM Mg(OAc)₂ as indicated. (A) Cleavage of pPKC₉G₃₃ and pPKC₉G₃₃ (G₇₄) with *Eco* RPR_{wt} and *Eco* RPR_{C293} and cleavage of substrates carrying dC₉ and dU₉ with *Eco* RPR_{wt} as indicated. The experiments were performed at 37°C in buffer C and 800 mM Mg(OAc)₂. The substrate concentration was ≤0.02 μM, *Eco* RPR concentration 6.4 μM (lanes 2, 3, 5, 6, 8, 14 and 16) and 13 μM (lanes 10 and 12). Time of incubations: lanes 1–6, 300 min, lanes 7–12 and 15–16, 360 min, and lanes 13 and 14, 60 min. nts mark the size of products generated after cleavage at sites c0 (9 nt), m-1 (8 nt) and m+3 (11 nt). (B) Frequency of cleavage of pPKC₉G₃₃ at m-1 with *Eco* RPR_{wt} and *Eco* RPR_{C294} in the absence of C5. The substrate and RPR concentrations were ≤0.02 μM and 9.6 μM and the reactions were as described in Materials and Methods, and panel A. Time of incubation, 90 min. The frequencies represent the mean and experimental errors of at least three independent experiments, see also Figure legend 2, panel C.

m-1 site as discussed above. In the few instances where the ‘G₁₀-A₁₁-U₆₉’ configuration was observed, the orientation of N₉ (N = A, G or U) is such that its phosphate group does not point in the right direction for cleavage to occur. These data are consistent with the orientation of N₉ (N₋₁ in pre-tRNAs and model substrates) being generally dependent on base identity at this position (see [25,51] and **Supplemental Figure S2**; S2A and S2B).

Docking the original biotin-binding RNA aptamer (pPK) into the reactive centre in the RNase P-tRNA crystal (Figure S2C) and cryo-EM *Eco* RNase P-pre(A₋₂U₋₁)-tRNA (Fig S2D) structures [50,51] by superimposing the G₁₀-C₃₂ pseudoknot and G₁-C₇₂ tRNA base-pairs show that pPK fit into the pocket. Also, the pre-tRNA and pPK scissile phosphates occupy overlapping positions (marked with a black arrow in Fig S2D; note, the RNase P-tRNA crystal structure represent the post-cleavage state [50]). We note that there is also space for the added 5'-GCCAC 3' trailer needed for the establishment of the RCCA-RPR interaction and cleavage of the pseudoknot RNA (see above). One difference comparing the interaction with pre(A₋₂U₋₁)-tRNA and pPK is the stacking between residues in the pre(A₋₂U₋₁)-tRNA 5' leader and residues in the RPR while A₉ and C₈ in the pseudoknot RNA do not stack on RPR residues in keeping with our modelling studies. Another is that A₉ and C₈ point in the opposite direction relative to U₋₁ and A₋₂ in the pre-tRNA. Finally, RPR residues positioned in the vicinity of the pPKN₉G₃₃

cleavage sites in the modelled structures discussed above are also observed in the RNase P-tRNA crystal and cryo-EM *Eco* RNase P-pre(A₋₂U₋₁)-tRNA structures (for comparison cf. **Figures 6 and 8**, and **Supplemental Figure S2**) [50,51].

Impact of *Eco* RPR residue 332 on cleavage site selection

The modelling discussed above suggested that residue G₃₃₂ (*Eco* RPR numbering; **Figure 7**) interacts with C₉ (but not when N₉ = A, G or U) in pPKC₉G₃₃ for cleavage at the m-1 site (**Figure 6C**). Hence, we substituted G₃₃₂ in *Eco* RPR with A, C and U to further understand its role in site selection in cleavage of pPKC₉G₃₃. Changing G to U at 332 increased the frequency of pPKC₉G₃₃ cleavage at m-1 (**Figure 9A**, cf. lanes 10 and 7–9) while A or C mutations at position 332 in the RPR did not affect site selection to any significant extent relative to wild-type *Eco* RPR with G₃₃₂ (**Figure 9A and B**). Determinations of the rate constant, k_{app}, revealed that the increased cleavage at m-1 is attributable to an almost four-fold reduction in k_{app} for cleavage at the c0 site, while only a marginal effect was detected for cleavage at m-1 (cf. G₃₃₂ vs. U₃₃₂; **Table 2**). The modelling suggested that the guanosine (G₃₃₂) carbonyl oxygen, O-6, possibly forms an H-bond with the exocyclic amine of C₉ during m-1 cleavage (**Figure 6C**). Given that U₃₃₂ carries two carbonyl oxygens at positions 2 and 4 provides one possible reason for the increased

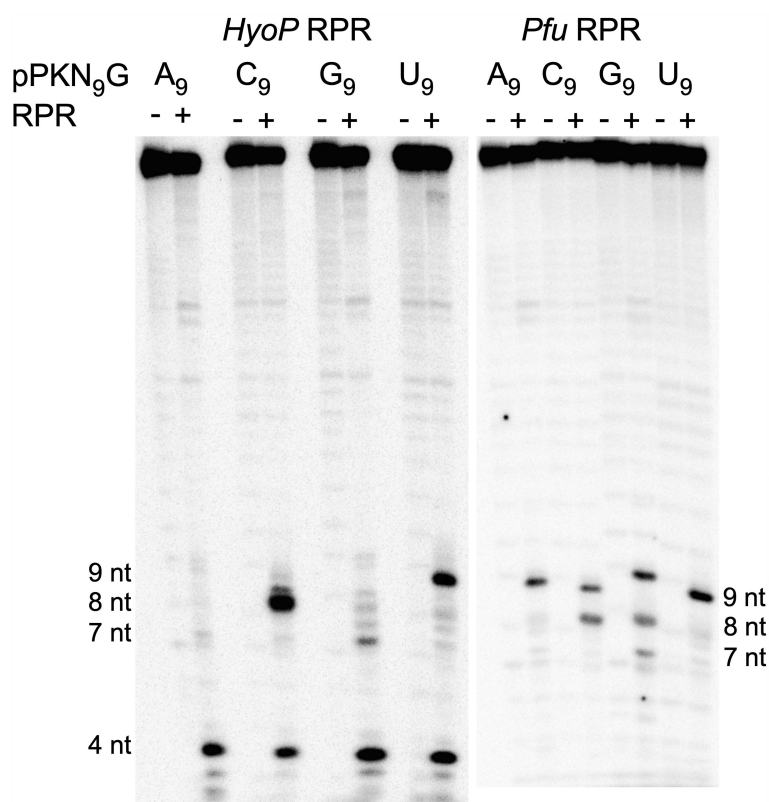


Figure 5. Cleavage of pPKN₉G₃₃ variants with *HyoP* RPR and *Pfu* RPR as indicated. 9, 8, 7 and 4 nt mark the size of the cleavage products as a result of cleavage at c0, m-1, m-2 and m-5 (between C₄ and G₅; Figure 1A). The reactions were performed without (-) and with (+) RPR for 300 min. The reactions were performed in buffer C and 800 mM Mg(OAc)₂ at 37°C and the concentrations of substrate and RPRs were ≤0.02 μM of the indicated pPK variants (A₉, C₉, G₉ and U₉). Enzyme concentrations were 4.4 μM (*HyoP* RPR; substrates C₉ and U₉), 12 μM (*HyoP* RPR; substrates A₉ and G₉), 15 μM (*Pfu* RPR; substrates C₉ and U₉) and 7.4 μM (*Pfu* RPR; substrates A₉ and G₉).

frequency of cleavage at m-1 by enabling H-bonding and ‘trapping’ C₉ thereby favouring the ‘G₁₀-A₁₁-U₆₉’ configuration. This is supported by the data where we modelled the U₃₃₂ variant in complex with the pPKC₉G₃₃ substrate (Supplemental Figure S3A) and simulations indicating increased cleavage at the m-1 site for the U₃₃₂ compared to the other variants (Supplemental Figure S3B).

Discussion

RNase P cleaves several different types of RNA substrates, albeit involvement in the processing of pre-tRNAs is considered to be its main function in the cell. Here, we showed that a small RNA aptamer acts as a substrate for *Eco* RPR with and without the RNase P protein, C5, as well as for the type B *HyoP* RPR and the archaeal type A *Pfu* RPR. The RNA aptamer folds into an H-type pseudoknot structure and was selected for binding biotin [49,81; see also 48,82]. That RNase P cleaves RNA pseudoknots agrees with previously reported data [26–30]. However, the present study extends our understanding of the factors that contribute to cleavage of pseudoknot substrates, such as the importance of the N₉ identity, the RCCA-RPR interaction, and charge distribution and Mg²⁺ binding near the cleavage site. Together, our findings provide new insight into the structural architecture and positioning of Mg²⁺ at the cleavage site that influence the choice of cleavage site [see also 25].

The structural architecture at and in the vicinity of the cleavage site varies dependent on substrate

For *Eco* RPR, a C at N₉ resulted in cleavage at two positions, c0 and m-1, with almost equal frequencies, while the substrates with A, G or U at this position were cleaved preferentially at one site, c0 (between N₉ and G₁₀; Figure 1A). Our modelling studies suggested that cleavage at the alternative position m-1 depends on a configuration referred to as ‘G₁₀-A₁₁-U₆₉’, which is not favoured in pseudoknots with A, G or U at N₉. Residue G₃₃₂ (Figure 7) is predicted to stabilize this configuration through hydrogen bonding between the G₃₃₂ carbonyl oxygen O-6 and the C₉ exocyclic amine (2-NH₂-group; Figure 6C). Accordingly, our data revealed that replacing G₃₃₂ with U resulted in cleavage mainly at m-1 (the alternative cleavage site) supporting the importance of residue 332 with respect to the structural architecture at and in the vicinity of the cleavage site. It is conceivable that U₃₃₂ stabilizes the ‘G₁₀-A₁₁-U₆₉’ configuration through hydrogen bonding between the U₃₃₂ carbonyl oxygen O-4 and the 4-amino group of C at the N₉ position more efficiently than G₃₃₂. This would provide a rationale for the observed increase in cleavage at the alternative site m-1 with *Eco* RPR_{U332}. In this context, we note that cross-linking data position G₃₃₂ in close proximity of the 5’ terminal G in tRNA [83] and the U₋₁ (U₋₁/N₋₁ corresponds to N₉ in pPKN₉G₃₃) in a model pre-tRNA [84,85]. Also, the positioning of G₃₃₂ in bacterial RNase P-pre-tRNA cryo-EM structures depends on the identities of

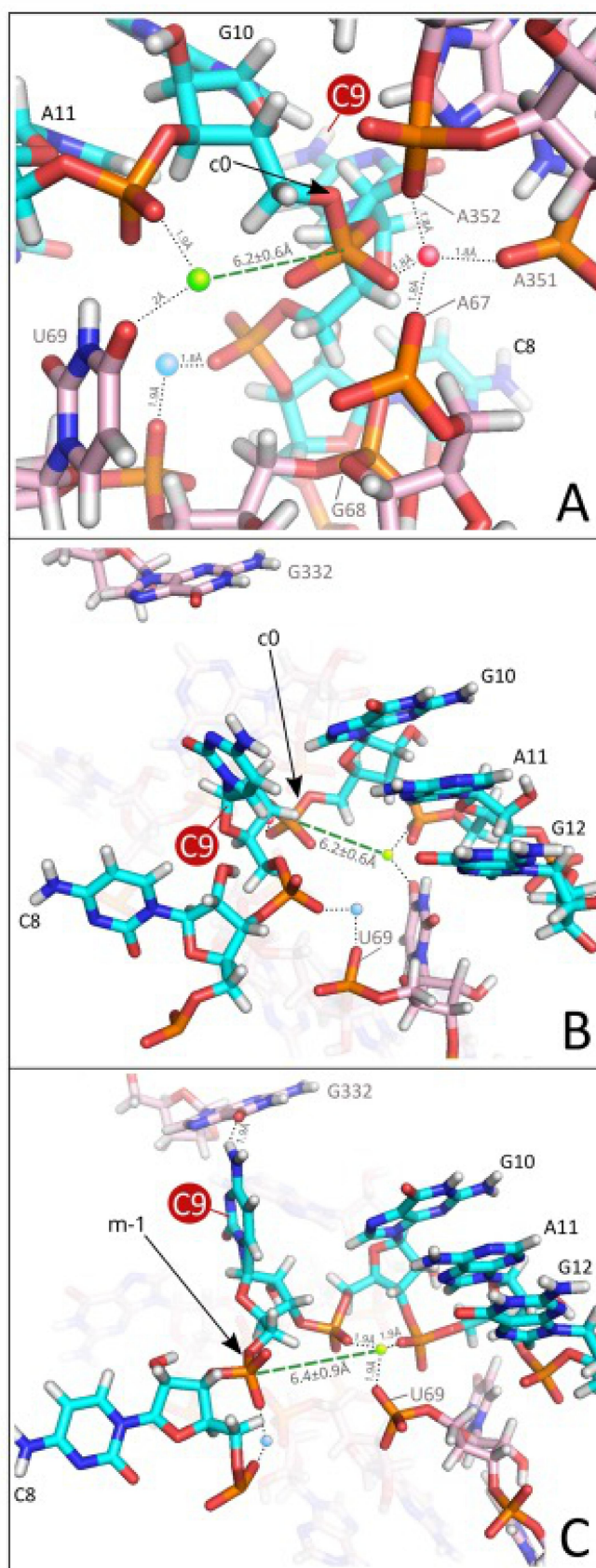
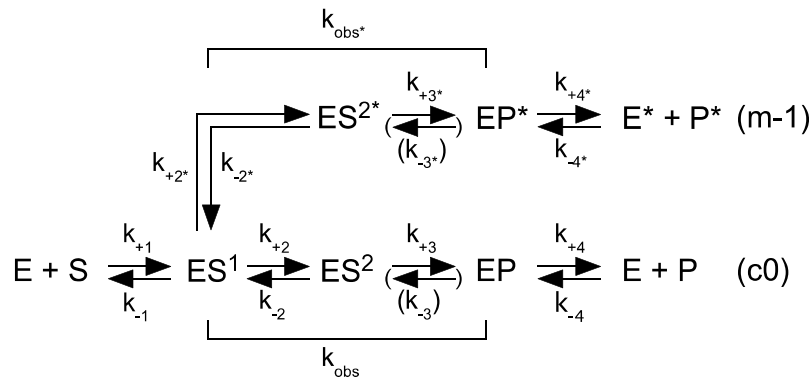


Figure 6. Modelling of RNase P RNA (RPR) in complex with pPKC₉G₃₃. (A) Canonical cleavage conformation displaying an inline nucleophilic attack by the Mg²⁺-activated H₂O (green dashed line). Functional groups in the Mg²⁺ (marked in green) ligand sphere include the phosphate group linked to A₁₁ (in pPKC₉G₃₃) and O-4 of U₆₉ (*Eco* RPR numbering, U₆₉ corresponds to U₅₂ in the RNase P-tRNA structure [50]). The black arrow marks the phosphate resulting in cleavage at the canonical site c0. In this model, binding between pPKC₉G₃₃ and RPR is also mediated by a second Mg²⁺ (marked in red) surrounded by phosphate groups linked to residue G₁₀ in the substrate and RPR residues A₆₇, A₃₅₁, and A₃₅₂. (B) Alternative view of the canonical cleavage site, c0 (marked with a black arrow), and location of the Mg²⁺ (marked in green) that activates the H₂O that acts as the nucleophile. Results shown in panels A and B are from the same simulation run. (C) Alternative cleavage conformation where the Mg²⁺ (marked in green) positioned for an in-



Scheme 1

N_{-2} and N_{-1} in the pre-tRNA 5' leader (Figure S2A, B) [51]. Together, this raises the possibility that G_{332} interacts similarly with other substrates carrying a C immediately 5' of canonical cleavage sites as observed in the pseudoknot substrates. For example, in mycobacteria, pre-tRNAs with C at the N_{-1} position are abundant [86], which might have an impact on the RNase P processing step. However, whether this affect cleavage site selection of native pre-tRNAs warrants for further studies.

The universally conserved bulged U_{69} (*Eco* RPR numbering; U_{52} in the RNase-tRNA structural complex; Figure 7) [50]; is also positioned close to pPKN₉G₃₃ cleavage sites and the Mg^{2+} predicted to generate the water nucleophile in our modelling. The importance of U_{69} is in keeping with previous reports [50, 87–99]. Moreover, the mechanism of RNase P-mediated cleavage is evolutionary conserved [40,50, 100–102] and in the recent cryo-EM structure of yeast RNase P in complex with a pre-tRNA A_{91} , U_{92} and U_{93} (yeast numbering) are positioned near the scissile phosphate, where U_{92} corresponds to U_{69} in *Eco* RPR [100]. In the bacterial RNase P-tRNA and RNase P-pre-tRNA structures U_{69} is also positioned near the canonical cleavage site [51,98]. Together this lends support to the validity of our modelling. Previous data further suggested that in cleavage of pre-tRNA by bacterial RPR, the U_{69} carbonyl oxygen O-4 coordinates Mg^{2+} , and modelling suggested that this Mg^{2+} activates the water that acts as the nucleophile [99, and references therein]. This is also one outcome of our modelling studies of cleavage of pPKC₉G₃₃ at the c0 site (Figure 6B) while for cleavage at m-1 our modelling data suggest that the *RpO* of U_{69} fulfils this role (Figure 6C).

Earlier, we reported the influence of the identity of residue N_{-1} on site selection and the kinetics of cleavage using a model hairpin substrate, pMini3bp (Figure 1E). The pMini3bp substrates used in these studies [23,25] and the pPKN₉G₃₃ variants are of similar size, and they cannot interact with the RPR region that binds the ‘T-stem-loop’ of pre-tRNAs [22,50,103]. Albeit both these substrates are cleaved preferentially at the junction of double and single-stranded

regions, the structural organization of their respective 5' leaders differ. Comparing the impact of the N_{-1}/N_9 identity on cleavage reveals striking differences (here we only compare the substrates having $A_{-1(9)}G$, $C_{-1(9)}G$, $G_{-1(9)}G$, $U_{-1(9)}G$ and $U_{-1(9)}A$; cf. Figure 1A, E). The pPKN₉G₃₃ substrates bind with 10-fold higher affinities to *Eco* RPR_{wt} compared to the corresponding pMini3bp variants with ‘ $G_{-1(9)}G$ ’ being the poorest binder for both substrate types. The improved binding might be attributed to that the structure of the pPKN₉G₃₃ ‘5’-leader’, with its two unpaired residues, displays a more defined and pre-organized structure compared to the more flexible pMini3bpN₋₁G 5' leader (Figure 1A, E); cf. K_d values in Table 1 vs. Table 1 in Ref [23] and might be related to that the entropic penalty for binding to the RPR is reduced for the pPKN₉G₃₃.

According to the simplified reaction scheme 1, following initial binding ES^1 undergoes a conformational change prior to cleavage [see e.g. Refs 23,78; see also Ref 104 and references therein]. The pMini3bp substrates are cleaved with higher efficiencies than the pPKN₉G₃₃ variants. The k_{obs} values for pMini3bpN₋₁G vary between 4.2 min^{-1} (‘ $U_{-1}G$ ’) and 0.0088 min^{-1} (‘ $G_{-1}G$ ’), which is almost 500-fold lower than k_{obs} for the ‘ $U_{-1}G$ ’ variant (Table S1 and Ref 23). For the pPKN₉G₃₃ variants, we detected approximately a 10-fold difference in k_{obs} with the highest values for the variants having U at N_9 (Table 1 and S1; pPKU₉G₃₃ and pPKU₉A₃₃; noteworthy, U is also present 5' of the RNase P cleavage site in the TYMV tRNA-like structure, another pseudoknot substrate) [30]. Hence, the difference in k_{obs} for the pPKN₉G₃₃ variants relative to the pMini3bpN₋₁G vary between 350- (U_{-1} vs. U_9) and 7-fold (G_{-1} vs. G_9). Using the k_{obs} values and $\Delta\Delta G = -RT\ln(k_{obs}pPKN_9G_{33}/k_{obs}(pMini3bpN_{-1}G))$ [105] this amounts to a difference of 2.2 to 3.6 kcal (comparing the A_{-1}/A_9 , U_{-1}/U_9 and C_{-1}/C_9 variants) and 1.2 kcal comparing the G_{-1}/G_9 variants (Table S1) in stabilization of the transition states. This would be in keeping with higher activation barriers for the pPKN₉G₃₃ relative to the pMini3bpN₋₁G variants that might be linked to the more defined and pre-organized structures of the ‘5’-leaders’ of the pPKN₉G₃₃

Escherichia coli RNase P RNA
(*Eco* RPR/ M1 RNA)

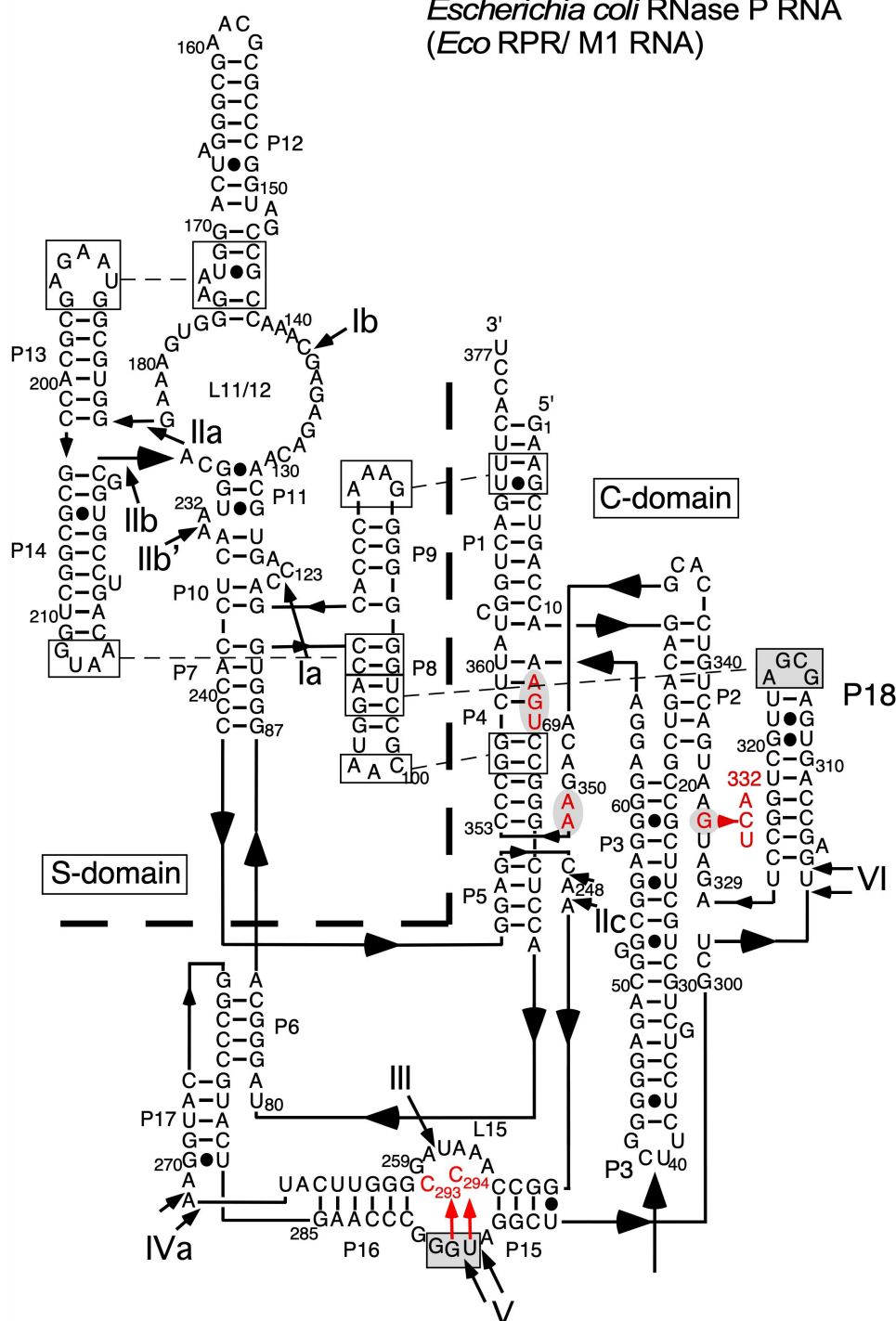


Figure 7. Structure model of type A *Eco* RPR according to Massire et al. [76]. Residues A₆₇, G₆₈, U₆₉, G₃₃₂, A₃₅₁ and A₃₅₂ (see main text and Figure 6) are marked in red on a grey background. The changes introduced at position 332 and in L15 are marked with red arrow (see also Figure 1C). For orientation the Pb²⁺-induced cleavage sites are included and indicated with roman numerals, see also [70,77]. The dashed line marks the demarcation between the S- and the C-domains.

variants (see also Figure S2). Also, the identity of the pMini3bp N₋₁ residue has a larger impact on transition state stabilization than in cleavage of the pPKN₉G₃₃ variants (larger variation in $\Delta\Delta G$ values for pMini3bp relative to pPKN₉G₃₃; Table S1). In this context, cleavage of both pre-tRNA and model hairpin substrates show that structured 5' leaders and base-pairing between residues N₋₂ (and/or N₋₁) and the first

C residue in the CCA-motif and/or the discriminator base influence cleavage rates [25, 106–108].

From our data, it is also apparent that addition of the C5 protein did not affect site selection except in the case of pPKC₉G₃₃ where we detected a small decrease of cleavage at m-1 relative to cleavage without C5 (Figure 2C). This is in contrast to cleavage of, for example, pMini3bpG₋₁G, which is cleaved \approx 40% at

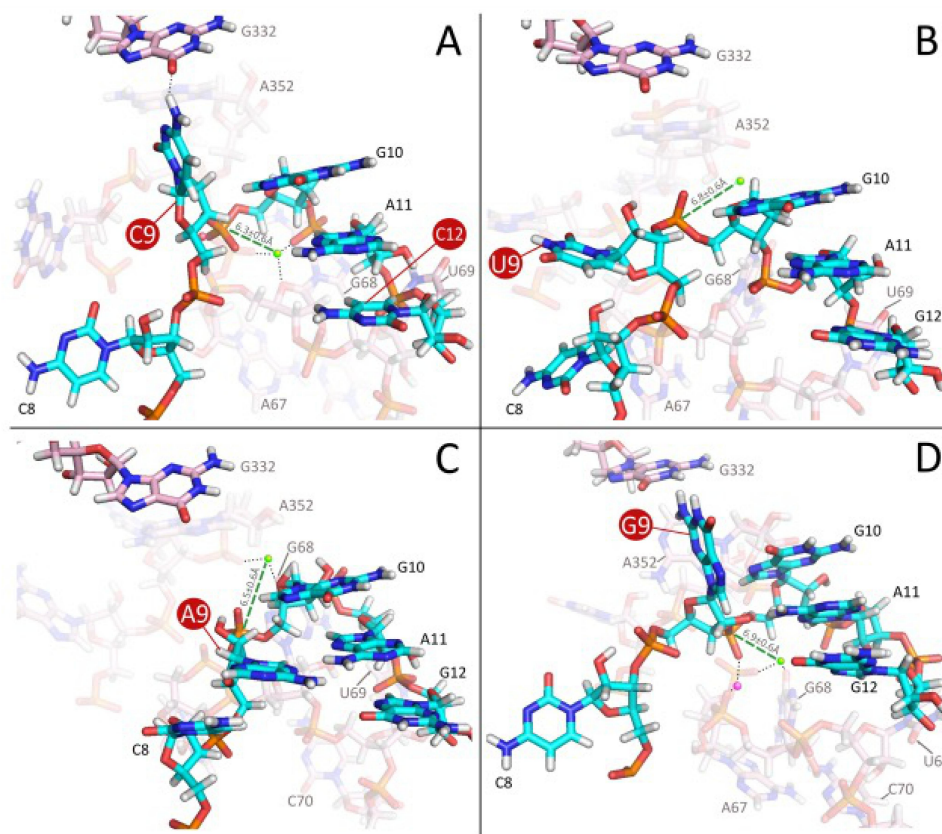


Figure 8. Modelling of RNase P RNA (RPR) in complex with four pPKN₉G₃₃ variants. (A) pPKC₉G₃₃91 in which G₁₂/C₃₀ was replaced with C₁₂/G₃₀. The replacement disturbs the position and binding patterns of Mg²⁺ (marked in green) positioned in the vicinity, creating a scenario where the G₁₀-A₁₁-U₆₉-Mg²⁺ configuration required for cleavage at the alternative m-1 site is energetically less favourable. (B-D) pPKU₉G₃₃ (B), pPKA₉G₃₃ (C) and pPKG₉G₃₃ (D). The spatial orientation of the C₈ and N₉ side chains for the U₉, A₉, and G₉ variants leads to: (i) conformation of the N₉ phosphate group incompatible with cleavage at the alternative m-1 site and (ii) RPR-pPKN₉G₃₃ binding conformation distinct from the G₁₀-A₁₁-U₆₉-Mg²⁺ configuration associated with cleavage at the alternative m-1 site. Pink- and cyan-coded nucleotides represent residues in the RPR and pPKN₉G₃₃, respectively. Coloured (green and pink; the Mg²⁺ generating the nucleophile are marked in green) spheres mark the positions of Mg²⁺ near the cleavage site, c0. For clarity, other residues belonging to the complex were omitted.

m-1 without C5 and almost exclusively at c0 with C5 (cf. [Figure 2E and F](#)) in [23]. Addition of C5 also suppresses cleavage of pre-tRNA^{Ser}Su1 at m-1 (*i.e.* -1) with *Eco* RPR variants that cannot establish a productive RCCA-RPR interaction [108]. (Noteworthy, the wt pre-tRNA^{Ser}Su1 carries a C at N₋₁; for impact of C5 on site selection using other pre-tRNAs see also e.g. [35,107,109]). The C5 protein interacts with N₋₈ - N₋₃ in the ‘single-stranded’ 5’ leaders [63,110,111]. Given that N₋₇ - N₋₃ are part of helix 1 in the pPKN₉G₃₃ substrates, it is unlikely that C5 binds to these residues (see e.g. [Figure 1](#) and S2D) as observed for N₋₁ and N₋₂ in the *Eco* RNase P-pre-tRNA cryoEM structures [51]. We also emphasize that pMini3bpG₋₁G was cleaved both at c0 and m-1 (+1 and -1, respectively) with almost equal frequencies (cf. [Figure 2](#)) in [23], while pMini3bpC₋₁G was cleaved mainly at c0 (+1). This is opposite to what we found using pPKG₉G₃₃ and pPKC₉G₃₃, which were cleaved mainly at c0 (pPKG₉G₃₃) and both at c0 and m-1 (pPKC₉G₃₃) ([Figure 2B](#)). Taken together, these differences might be related to the distinct structural organization of the 5’ leader and the architecture of the two types of substrates, which changes the role of the leader in substrate docking and formation of active site architecture (see also [Figure S2D](#)).

The RCCA-RPR interaction plays an important role for site selection in cleavage of pre-tRNA and model substrates [64,65,112]. The R residue corresponds to the discriminator

base at position 73 in tRNA (see above), and it pairs with U₂₉₄ in the *Eco* RPR-substrate complex and is referred to as the +73/294-interaction ([Figure 1D](#) [50,71]). Site selection in cleavage of the pseudoknot substrate pPKN₉G₃₃ (in particular pPKC₉G₃₃) also depends on the structural topography of the RCCA-RPR and +73/294-interactions (this study). This is consistent with previous findings, where different pre-tRNAs and model substrates were used [37,71,112]. In this context, we note that based on studies using variants of plant tRNA-like structures it was proposed that residues at -1 and +73 are important for efficient cleavage [30]. These authors also observed cleavage of pseudoknot substrates having a pyrimidine or purine at the position corresponding to N₋₁₍₉₎ but a deeper analysis of this finding was not done. Together, this suggests that the structural topography of the distant RCCA-RPR interaction has an impact on site selection and catalysis irrespective of substrate. In this context, the N₉ residue is most likely not in position to pair with residue G₃₃ that corresponds to the tRNA discriminator base in pPKN₉G₃₃ ([Figure 1A-C](#)). However, we cannot entirely exclude pairing between C₉ and G₃₃. Nevertheless, the RCCA-RPR interaction anchors

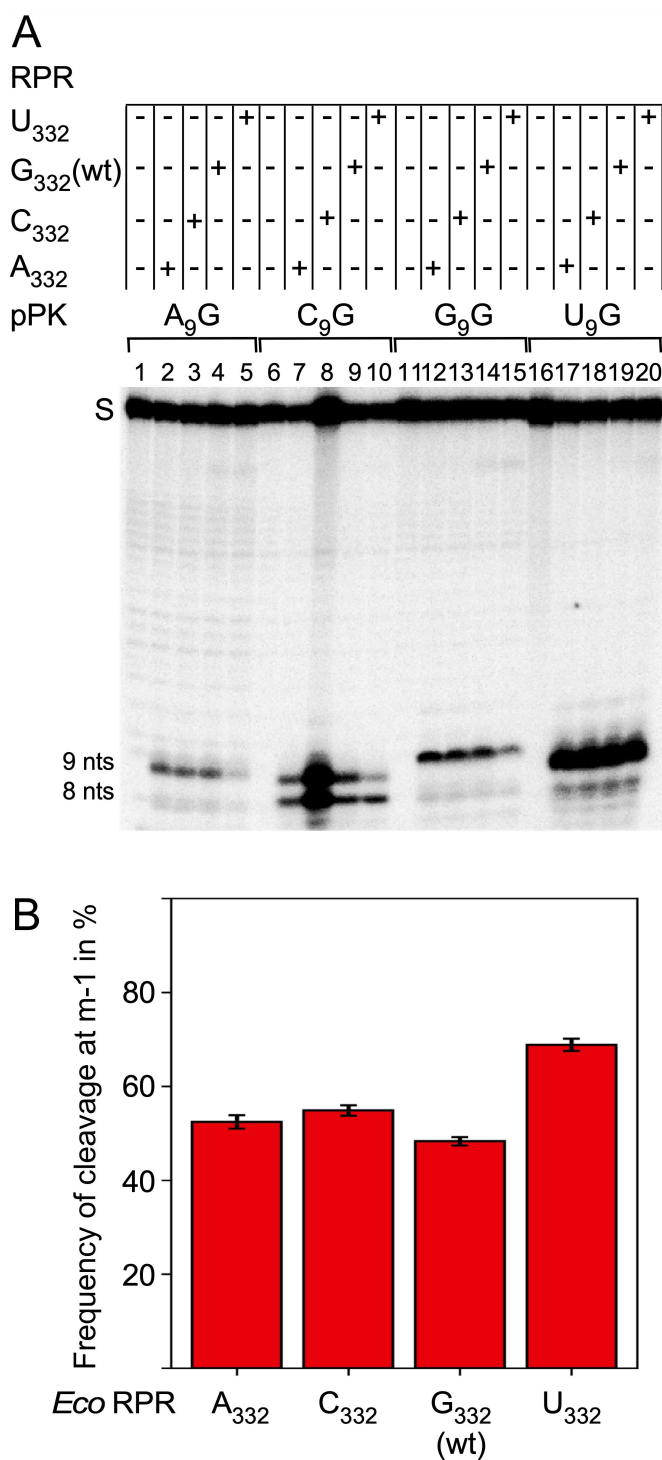


Figure 9. Cleavage of pPKN₉G₃₃ variants with *Eco* RPR 332 derivatives as indicated. (A) Lanes 1, 6, 11 and 16 correspond to reactions performed without RPR while the results of cleavage with the different RPR variants are presented in the other lanes as indicated. The reactions were performed in buffer C and 800 mM Mg(OAc)₂ at 37°C as described in Materials and Methods and in Figure legends 2, 4 and 5. The concentration of substrate was ≤ 0.02 μ M and *Eco* RPR concentrations were: lanes 7–10 and 17–20, 4.8 μ M, and lanes 2–5 and 12–15, 9.6 μ M. Time of incubation, 60 min. (B) Frequency of cleavage of pPKN₉G₃₃ at c0 and at m-1 with *Eco* RPR_{wt} and *Eco* RPR_{C294} in the absence of C5. The substrate and RPR concentrations were ≤ 0.02 μ M and 4.8 or 9.6 μ M and the reactions were as described in Materials and Methods. The frequencies represent the mean and experimental errors of at least three independent experiments, see also Figure legend 2B.

the substrate: conceivably it affects the structure near the cleavage site and thereby influencing the positioning of catalytic Mg²⁺-ion(s) (see also [37,64,71,112]).

In summary, our data support a model where the structural architecture at, and in the vicinity of, the cleavage site varies dependent on substrate with N₋₁₍₉₎ having a key role. As a consequence, and in addition to the impact of the RCCA-RPR interaction, this would influence the positioning of Mg²⁺ involved in generating the water nucleophile and/or stabilization of the developing oxyanion in the transition state. In this context, we previously reported that structurally different cleavage sites are aligned differently in the *Eco* RPR ‘active site’ [84,85; see also 25].

The structural architecture at, and in the vicinity of, the cleavage site has an impact on positioning of Mg²⁺ important for catalysis

RPR-mediated cleavage depends on divalent metal ions and considering both efficiency and site selection, Mg²⁺ is preferred ([70]; for a review see [39]). In the bacterial RNase P-tRNA and RNase P-pre-tRNA complexes, two Me²⁺-ions are positioned near the tRNA 5’ terminal phosphate [50,51,113,114]. Hence, it is likely that these are involved in generating the water nucleophile and transition state stabilization [98]. Two Mg²⁺ are also positioned close to ‘A₉G₁₀’ in pPK (without the 5’-GCCAC trailer; Figure 1B, C) and one in the vicinity of the corresponding residues in the TYMV tRNA-like structure [47,49]. In keeping with this, our unpublished data show that both Pb²⁺ and Mg²⁺ induce cleavage at positions near N₉ in the pPKN₉G₃₃ variants consistent with the presence of Mg²⁺ at this location (not shown). Hence, in the case of pPKA₉G₃₃, one or both Mg²⁺ are positioned such that they might take part in catalysis (see also our modelling data above). In this context, we note that based on Me²⁺-induced cleavage data with both pre-tRNA and model hairpin substrates, it was suggested that a substrate coordinating a Mg²⁺ near the cleavage site is the true substrate for RNase P [73,115,116].

Cleavage of pPKC₉G₃₃ required a higher concentration of Mg²⁺ for optimal cleavage compared to the other N₉ variants. By changing the orientation of base pairs in helix 2 (see pPKC₉G₃₃ ‘91–93’ variants) alter the chemical groups of the bases facing C₉ and hence would affect the charge distribution in the vicinity of the cleavage site (Figure 1B, C). These changes resulted in lower Mg²⁺ requirement to reach optimal cleavage rates and increased the frequency of cleavage at the c0 site. Also, this resulted in an 80% reduction in the number of dynamical modelling runs compatible with the ‘G₁₀-A₁₁-U₆₉’ configuration (note that the Mg²⁺ generating the nucleophile in this configuration is coordinated differently, U₆₉ RpO vs. O-4, compared to cleavage at c0; Figure 6). Our data also showed that the cleavage site shifts in response to the addition of Mn²⁺ and Sr²⁺, which is in keeping with previous data [34,70,71]. Together, these data are consistent with a model where one (or both) of the Mg²⁺

Table 2. The rate constant k_{app} for cleavage of pPKC₉G₃₃ with *Eco* RPR 332 variants at 800 mM Mg²⁺.

Substrate	Cleavage site	k_{app} (min ⁻¹ pmol ⁻¹)
<i>Eco</i> RPR _{G332} (wt)	c0	$(57 \pm 7.7) \times 10^{-3}$
	m-1	$(49 \pm 7.6) \times 10^{-3}$
<i>Eco</i> RPR _{A332}	c0	$(42 \pm 5.3) \times 10^{-3}$
	m-1	$(46 \pm 6.1) \times 10^{-3}$
<i>Eco</i> RPR _{C332}	c0	$(30 \pm 2.6) \times 10^{-3}$
	m-1	$(36 \pm 0.31) \times 10^{-3}$
<i>Eco</i> RPR _{U332}	c0	$(16 \pm 1.7) \times 10^{-3}$
	m-1	$(34 \pm 0.27) \times 10^{-3}$

The experiments were performed under saturating single turnover conditions at 800 mM Mg²⁺ at pH 6.1 as described in Materials and Methods. The concentrations of *Eco* RPR and substrate were 0.8 and ≤ 0.02 μ M, respectively. The data represent mean \pm experimental errors calculated from at least three independent experiments.

is positioned near 'A₉G₁₀' in pPK participate in catalysis ([39,50]; Figure 1B, C). Moreover, altering the structural architecture, such that the aforementioned charge distribution is changed, influences positioning of this (or these) Mg²⁺ ions. In this context, we emphasize that substituting residues in the T-loop of yeast tRNA^{Phe} affects the positioning of Pb²⁺ (such that Pb²⁺ hydrolysis in the D-loop is affected) [79, 117–119].

As for other substrates, the 2'-OH immediately 5' of the cleavage sites plays an important role for cleavage at this position. For pPKC₉G₃₃, introducing a 2'-H at C₉ shifted cleavage to the alternative site m-1 while having a 2'-H at C₈ resulted in cleavage preferentially at c0. This is in contrast to what would be predicted on the basis of the 2'-OH model, which states that the RPR binds the 2'-OH at N₋₁ in pre-tRNAs and influences cleavage at other positions [120,121]. However, the influence of changing the 2'-OH to 2'-H at N₉ depends on the base identity since the pPKdU₉G₃₃ variant did not abolish cleavage at c0 (but it was significantly reduced) and cleavage was detected at a new site, the m+3 site in helix 2, but notably not at m-1 (Figure 4; see also [25,75] for discussion). On the basis of this finding, it is unlikely that changing the U₉ 2'-OH to 2'-H promotes the formation of the 'G₁₀-A₁₁-U₆₉' configuration, which according to our modelling is associated with cleavage at the m-1 site (see above). We and others have argued that the 2'-OH at N₋₁ acts as an inner or outer sphere for Mg²⁺ binding at the cleavage site, thereby affecting substrate binding and catalysis ([34,37] but see [36] for an alternative model). Thus, changing the 2'-OH to 2'-H would likely change the structural architecture at the cleavage site, resulting in a shift in the positioning of Mg²⁺, which leads to cleavage at alternative sites.

Concluding remarks

In many plant RNA viruses, the tRNA-like structure at the 3' termini is amino-acylated. For the TYMV virus, valylation is required for its amplification and enhancement of gene expression. It has been discussed that the valylation of the 3' termini has a role in regulation of gene expression vs. replication of the positive strand, for a review see [122]. *In vitro* studies show that RNase P cleaves TYMV RNA and generate a fragment that includes the 3' terminus [28–30]. Hence, this raises the possibility that this cleavage event is one step in this regulatory circuit by affecting enhancement of gene expression and amplification.

In this context, it might be possible to adapt the EGS or the MIGS technology [123 and references therein] to develop ribozymes that cleave the TYMV 3' end (or the 3' end of other RNA plant virus) efficiently and use these to influence/prevent virus amplification and gene expression *in vivo*.

Apart from having a possible role in releasing the 3' terminal tRNA-like structure from certain RNA viral genomes, pseudoknots present in mRNAs might be potential targets for RNase P as well. RNase P has been reported to process/influence processing of several mRNAs [11,14,20,24 and unpublished data] and whether the cleavage sites in these mRNAs is linked to pseudoknots is not known but one mRNA, the T2 and T4 bacteriophage gene 32 mRNA, is of particular interest. This mRNA is claimed to be a substrate for RNase P [30] and it contains a pseudoknot structure of the H-type followed by a 3' ACCA sequence [42–44]. Whether RNase P recognizes this pseudoknot (and other pseudoknot structures embedded in mRNAs) and cleaves it in accordance with our present data, and those reported by others, warrants further studies. Here, binding of biotin to pseudoknots might be one tool to use in the process of identifying pseudoknot structures.

Finally, we note that cleavage by PRORP1 (proteinous RNase P-like activity) is affected by the N₋₁ identity with C₋₁ resulting in cleavage at -1 [124–126]. Given that the structures of substrates near the cleavage site vary, this implies that the structural architecture of the PRORP active sites change in a substrate-dependent manner and that N₋₁ has a key role. It would therefore be interesting to understand whether specific active site configurations influence the choice of cleavage site also in PRORP-mediated cleavage.

Acknowledgments

We thank our colleagues for discussions throughout this work, Dr AC Forster for critical reading of the manuscript, Dr D Larsson for assistance generating Figures S2C and D, and Dr J Åqvist for discussions. We also acknowledge the constructive comments by the reviewers. This work was supported by the Swedish Research Council (N/T) and the Uppsala RNA Research Center (Swedish Research Council Linneus support). The computations were performed on resources provided by SNIC through Uppsala Multidisciplinary Center for Advanced Computational Science (UPPMAX) under Project SNIC 2015/7-30.

Disclosure statement

No potential conflict of interest was reported by the author(s).

Funding

This study was funded by the Swedish Research Council [Grant ID PI Kirsebom: 2016-04602; 621-2011-5848 and Linneus Grant to Uppsala RNA Research Center Grant ID 349-2006-267].

Data availability

The MMB executable is available as a docker container, which can be pulled as samuelflores/mmb-ubuntu, while the code is available at <https://github.com/samuelflores/MMB>. The input files created for this work are available at https://github.com/LLN273/RNaseP_pseudoknot.

All data and materials are available from the corresponding author.

References

- [1] Liu F, Altman S. Ribonuclease P. Protein reviews. Vol. 10. New York Dordrecht Heidelberg London: Springer; 2010.
- [2] Guerrier-Takada C, Gardiner K, Marsh T, et al. The RNA moiety of ribonuclease P is the catalytic subunit of the enzyme. *Cell*. 1983;35(3):849–857.
- [3] Pannucci JA, Haas ES, Hall TA, et al. RNase P RNAs from some archaea are catalytically active. *Proc Natl Acad Sci USA*. 1999;96(14):7803–7808.
- [4] Tsai H-Y, Pulkunat DK, Woznick WK, et al. Functional reconstitution and characterization of pyrococcus furiosus RNase P. *Proc Natl Acad Sci USA*. 2006;103(44):16147–16152.
- [5] Kikovska E, Svård SG, Kirsebom LA. Eukaryotic RNase P RNA mediates cleavage in the absence of protein. *Proc Natl Acad Sci USA*. 2007;104(7):2062–2067.
- [6] Holzmann J, Frank P, Löffler E, et al. RNase P without RNA: identification and functional reconstitution of the human mitochondrial tRNA processing enzyme. *Cell*. 2008;135(3):462–474.
- [7] Gobert A, Gutmann B, Taschner A, et al. A single Arabidopsis organellar protein has RNase P activity. *Nat Struct Mol Biol*. 2010;17(6):740–744.
- [8] Lai LB, Bernal-Bayard P, Mohannath G, et al. A functional RNase P protein subunit of bacterial origin in some eukaryotes. *Mol Genet Genomics*. 2011;286(5–6):359–369.
- [9] Taschner A, Weber C, Buzet A, et al. Nuclear RNase P of *Trypanosoma brucei*: a single protein in place of the multicomponents RNA-protein complex. *Cell Rep*. 2012;2(1):19–25.
- [10] Nickel AI, Wäber NB, Gößringer M, et al. Minimal and RNA-free RNase P in *Aquifex aeolicus*. *Proc Natl Acad Sci USA*. 2017;114(42):11121–11126.
- [11] Bothwell ALM, Stark BC, Altman S. Ribonuclease P substrate specificity: cleavage of a bacteriophage Φ 80-induced RNA. *Proc Natl Acad Sci USA*. 1976;73(6):1912–1916.
- [12] McClain WH, Guerrier-Takada C, Altman S. Model substrates for an RNA enzyme. *Science*. 1987;238(4826):527–530.
- [13] Forster AC, Altman S. External guide sequences for an RNA enzyme. *Science*. 1990;249(4970):783–786.
- [14] Alifano P, Rivellini F, Piscitelli C, et al. Ribonuclease E provides substrates for ribonuclease-dependent processing of a polycistronic mRNA. *Genes Dev*. 1994;8(24):3021–3031.
- [15] Komine Y, Kitabatake M, Yokogawa T, et al. A tRNA-like structure is present in 10Sa RNA, a small stable RNA from *Escherichia coli*. *Proc Natl Acad Sci USA*. 1994;91(20):9223–9227.
- [16] Hartmann RK, Heinrich J, Schlegl J, et al. Precursor of C4 antisense RNA of bacteriophages P1 and P7 is a substrate for RNase P of *Escherichia coli*. *Proc Natl Acad Sci USA*. 1995;92(13):5822–5826.
- [17] Pan T. Novel RNA substrates for the ribozyme from *Bacillus subtilis* ribonuclease P identified by in vitro selection. *Biochemistry*. 1995;34(26):8458–8464.
- [18] Kufel J, Kirsebom LA. The P15-loop of *Escherichia coli* RNase P RNA is an autonomous divalent metal ion binding domain. *RNA*. 1998;4(7):777–788.
- [19] Hansen A, Pfeiffer T, Zuleeg T, et al. Exploring the minimal substrate requirements for trans-cleavage by RNase P holoenzymes from *Escherichia coli* and *Bacillus subtilis*. *Mol Microbiol*. 2001;41(1):131–143.
- [20] Li Y, Altman S. A specific endoribonuclease, RNase P, affects gene expression of polycistronic operon mRNAs. *Proc Natl Acad Sci USA*. 2003;100(23):13213–13218.
- [21] Altman S, Wesolowski D, Guerrier-Takada C. RNase P cleaves transient structures in some riboswitches. *Proc Natl Acad Sci USA*. 2005;102(32):11284–11289.
- [22] Brännvall M, Kikovska E, Wu S, et al. Evidence for induced fit in bacterial RNase P RNA-mediated cleavage. *J Mol Biol*. 2007;372(5):1149–1164.
- [23] Wu S, Chen Y, Mao G, et al. Transition-state stabilization in *Escherichia coli* ribonuclease P RNA-mediated cleavage of model substrates. *Nucl Acids Res*. 2014;42(1):631–642.
- [24] Mohanty BK, Kushner SR. Inactivation of RNase P in *Escherichia coli* significantly changes post-transcriptional RNA metabolism. *Mol Microbiol*. 2022;117(1):121–142.
- [25] Mao G, Srivastava AS, Wu S, et al. Importance of residue 248 in *Escherichia coli* RNase P RNA mediated cleavage. *Sci Rep*. 2023;13(1):14140.
- [26] Prochiantz A, Haenni AL. TYMV RNA as a substrate of tRNA maturation endonuclease. *Nat New Biol*. 1973;241(110):168–170.
- [27] Silberklang M, Prochiantz A, Haenni A-L, et al. Studies on the sequence of the 3'-terminal region of turnip-yellow-mosaic-virus RNA. *Eur J Biochem*. 1977;72(3):465–478.
- [28] Green CJ, Vold BS, Morch MD, et al. Ionic conditions for the cleavage of the tRNA-like structure of turnip yellow mosaic virus by the catalytic RNA of RNase P. *J Biol Chem*. 1988;263(24):11617–11620.
- [29] Guerrier-Takada C, van Belkum A, Pleij CW, et al. Novel reactions of RNAase P with a tRNA-like structure in turnip yellow mosaic virus RNA. *Cell*. 1988;53(2):267–272.
- [30] Mans RM, Guerrier-Takada C, Altman S, et al. Interaction of RNase P from *Escherichia coli* with pseudoknotted structures in viral RNAs. *Nucl Acids Res*. 1990;18(12):3479–3487.
- [31] Kozak M. Regulation of translation via mRNA structure in prokaryotes and eukaryotes. *Gene*. 2005;361:13–37.
- [32] Atkins JF, Loughran G, Bhatt PR, et al. Ribosomal frameshifting and transcriptional slippage: from genetic steganography and cryptography to adventitious use. *Nucl Acids Res*. 2016;44(15):7007–7078.
- [33] Loria A, Pan T. Recognition of the T Stem-Loop of a Pre-tRNA Substrate by the Ribozyme from *Bacillus subtilis* Ribonuclease P. *Biochemistry*. 1997;36(21):6317–6325.
- [34] Persson T, Cuzic S, Hartmann RK. Catalysis by RNase P RNA: unique features and unprecedented active site plasticity. *J Biol Chem*. 2003;278(44):43394–43401.
- [35] Zahler NH, Christian EL, Harris ME. Recognition of the 5' leader of pre-tRNA substrates by the active site of ribonuclease P. *RNA*. 2003;9(6):734–745.
- [36] Zahler NH, Sun L, Christian EL, et al. The Pre-tRNA Nucleotide Base and 2'-Hydroxyl at N(-1) Contribute to Fidelity in tRNA Processing by RNase P. *J Mol Biol*. 2005;345(5):969–985.
- [37] Brännvall M, Kikovska E, Kirsebom LA. Cross talk between the +73/294 interaction and the cleavage site in RNase P RNA mediated cleavage. *Nucl Acids Res*. 2004;32(18):5418–5429.
- [38] Cuzic-Feltens S, Weber MHW, Hartmann RK. Investigation of catalysis by bacterial RNase P via LNA and other modifications at the scissile phosphodiester. *Nucl Acids Res*. 2009;37(22):7638–7653.
- [39] Kirsebom LA Roles of metal ions in RNase P catalysis In: Liu F, Altman S editors. *Protein Reviews Vol 10*. New York NY 10013: Springer Science+Business Media, LLC, 233 Springer Street; 2010. p. 113–134
- [40] Phan H-D, Lai LB, Zahurancik WJ, et al. The many faces of RNA-based RNase P, an RNA-world relic. *Trends Biochemical Sciences*. 2021;46(12):976–991.
- [41] Shen LX, Tinoco I. The structure of an RNA pseudoknot that causes efficient frameshifting in mouse mammary tumor virus. *J Mol Biol*. 1995;247(5):963–978.
- [42] Du Z, Giedroc DP, Hoffman DW. Structure of the autoregulatory pseudoknot within the gene 32 messenger RNA of bacteriophages T2 and T6: a model for a possible family of structurally related RNA pseudoknots. *Biochemistry*. 1996;35(13):4187–4198.
- [43] Du Z, Hoffman DW. An NMR and mutational study of the pseudoknot within the gene 32 mRNA of bacteriophage T2: insights into a family of structurally related RNA pseudoknots. *Nucl Acids Res*. 1997;25(6):1130–1135.
- [44] Kolka MH, van der Graaf M, Wijmenga SS, et al. NMR structure of a classical pseudoknot: interplay of single- and double-stranded RNA. *Science*. 1998;280(5362):434–437.
- [45] Theimer CA, Wang Y, Hoffman DW, et al. Non-nearest neighbor effects on the thermodynamics of unfolding of a model mRNA pseudoknot. *J Mol Biol*. 1998;279(3):545–564.

- [46] Wang Y, Wills NM, Du Z, et al. Comparative studies of frame-shifting and nonframeshifting RNA pseudoknots: a mutational and NMR investigation of pseudoknots derived from the bacteriophage T2 gene 32 mRNA and the retroviral gag-pro frameshift site. *RNA*. 2002;8(8):981–996.
- [47] Colussi TM, Costantino DA, Hammond JA, et al. The structural basis of transfer RNA mimicry and conformational plasticity by a viral RNA. *Nature*. 2014;511(7509):366–369.
- [48] Peselis A, Serganov A. Structure and function of pseudoknots involved in gene expression control. *Wiley Interdiscip Rev RNA*. 2014;5(6):803–822.
- [49] Nix J, Sussman D, Wilson C. The 1.3 Å crystal structure of a biotin-binding pseudoknot and the basis for RNA molecular recognition. *J Mol Biol*. 2000;296(5):1235–1244.
- [50] Reiter NJ, Osterman A, Torres-Larios A, et al. Structure of a bacterial ribonuclease P holoenzyme in complex with tRNA. *Nature*. 2010;468(7325):784–789.
- [51] Zhu J, Huang W, Zhao J, et al. Structural and mechanistic basis for recognition of alternative tRNA precursor substrates by bacterial ribonuclease P. *Nat Commun*. 2022;13(1):5120.
- [52] Svärd SG, Mattsson JG, Johansson KE, et al. Cloning and characterization of the RNase P RNA genes from two porcine mycoplasmas. *Mol Microbiol*. 1994;11(5):849–859.
- [53] Sinapah S, Wu S, Chen Y, et al. Cleavage of model substrates by archaeal RNase P: role of protein cofactors in cleavage-site selection. *Nucl Acids Res*. 2011;39(3):1105–1116.
- [54] Milligan JF, Groebe DR, Witherell GW, et al. Oligoribonucleotide synthesis using T7 RNA polymerase and synthetic DNA templates. *Nucl Acids Res*. 1987;15(21):8783–8798.
- [55] Feltens R, Gossringer M, Willkomm DK, et al. An unusual mechanism of bacterial gene expression revealed for the RNase P protein of *Thermus* strains. *Proc Natl Acad Sci USA*. 2003;100(10):5724–5729.
- [56] Flores SC, Altman RB. Turning limited experimental information into 3D models of RNA. *RNA*. 2010;16(9):1769–1778.
- [57] Flores SC, Wan Y, Russell R, et al. Predicting RNA structure by multiple template homology modeling. *Pac Sym Biocomput*. 2010;216–227.
- [58] Flores SC, Sherman MA, Bruns CM. Fast flexible modeling of RNA structure using internal coordinates. *Trans Comput Biol Bioinform*. 2011;8(5):1247–1257.
- [59] Flores SC. Fast fitting to low resolution density maps: elucidating large-scale motions of the ribosome. *Nucl Acids Res*. 2014;42(2):e9.
- [60] Caulfield T, Coban M, Tek A, et al. Molecular Dynamics Simulations Suggest a Non-Doublet Decoding Model of –1 Frameshifting by tRNA^{Ser3}. *Biomolecules*. 2019;18(11):745.
- [61] Koriipella RK, Holm M, Dourado D, et al. A conserved histidine in switch-II of EF-G moderates release of inorganic phosphate. *Sci Rep*. 2015;5(1):12970.
- [62] Tek A, Korostelev AA, Flores SC. MMB-GUI: a fast morphing method demonstrates a possible ribosomal tRNA translocation trajectory. *Nucl Acids Res*. 2016;44(1):95–105.
- [63] Niranjanakumari S, Stams T, Crary SM, et al. Protein component of the ribozyme ribonuclease P alters substrate recognition by directly contacting precursor tRNA. *Proc Natl Acad Sci USA*. 1998;95(26):15212–15217.
- [64] Kirsebom LA, Svärd SG. Base pairing between *Escherichia coli* RNase P RNA and its substrate. *EMBO J*. 1994;13(20):4870–4876.
- [65] Svärd SG, Kagardt U, Kirsebom LA. Phylogenetic comparative mutational analysis of the base-pairing between RNase P RNA and its substrate. *RNA*. 1996;2(5):463–472.
- [66] Wegscheid B, Hartmann RK. The precursor tRNA 3'-CCA interaction with *Escherichia coli* RNase P RNA is essential for catalysis by RNase P in vivo. *RNA*. 2006;12(12):2135–2148.
- [67] Wegscheid B, Hartmann RK. In vivo and in vitro investigation of bacterial type B RNase P interaction with tRNA 3'-CCA. *Nucl Acids Res*. 2007;35(6):2060–2073.
- [68] Pettersson BMF, Kirsebom LA. The presence of a C-1/G+73 pair in a tRNA precursor influences processing and expression in vivo. *J Mol Biol*. 2008;381(5):1089–1097.
- [69] Crothers DM, Seno T, Söll D. Is there a discriminator site in transfer RNA? *Proc Natl Acad Sci USA*. 1972;69(10):3063–3067.
- [70] Brännvall M, Kirsebom LA. Metal ion cooperativity in ribozyme cleavage of RNA. *Proc Natl Acad Sci USA*. 2001;98(23):12943–12947.
- [71] Brännvall M, Pettersson BMF, Kirsebom LA. Importance of the +73/294 interaction in *Escherichia coli* RNase P RNA substrate complexes for cleavage and metal ion coordination. *J Mol Biol*. 2003;325(4):697–709.
- [72] Kirsebom LA, Trobro S. RNase P RNA-mediated cleavage. *IUBMB Life*. 2009;61(3):189–200.
- [73] Perreault JP, Altman S. Important 2'-hydroxyl groups in model substrates for M1 RNA, the catalytic RNA subunit of RNase P from *Escherichia coli*. *J Mol Biol*. 1992;226(2):399–409.
- [74] Smith D, Pace NR. Multiple magnesium ions in the ribonuclease P reaction mechanism. *Biochemistry*. 1993;32(20):5273–5281.
- [75] Brännvall M, Kirsebom LA. Complexity in orchestration of chemical groups near different cleavage sites in RNase P RNA mediated cleavage. *J Mol Biol*. 2005;351(2):251–257.
- [76] Massire C, Jaeger L, Westhof E. Derivation of the three-dimensional architecture of bacterial ribonuclease P RNAs from comparative sequence analysis. *J Mol Biol*. 1998;279(4):773–793.
- [77] Ciesiolka J, Hardt W-D, Schlegl J, et al. Lead-ion-induced cleavage of RNase P RNA. *Eur J Biochem*. 1994;219(1–2):49–56.
- [78] Mao G, Srivastava AS, Kosek D, et al. Critical domain interactions for type A RNase P RNA-mediated catalysis with and without the specificity domain. *PLOS ONE*. 2018;13:e0192873.
- [79] Brown RS, Dewan JC, Klug A. Crystallographic and biochemical investigation of the lead(II)-catalyzed hydrolysis of yeast phenylalanine tRNA. *Biochemistry*. 1985;24(18):4801–4875.
- [80] Cowan JA. Metal activation of enzymes in nucleic acid biochemistry. *Chem Rev*. 1998;98(3):1067–1088.
- [81] Pleij CWA. Pseudoknots: a new motif in the RNA game. *Trends Biochem Sci*. 1990;15(4):143–147.
- [82] Brierley I, Pennell S, Gilbert RJC. Viral RNA pseudoknots: versatile motifs in gene expression and replication. *Nat Microbiol Rev*. 2007;5(8):598–610.
- [83] Burgin AB, Pace NR. Mapping the active site of ribonuclease P RNA using a substrate containing a photoaffinity agent. *EMBO J*. 1990;9(12):4111–4118.
- [84] Kufel J, Kirsebom LA. Different cleavage sites are aligned differently in the active site of M1 RNA, the catalytic subunit of *Escherichia coli* RNase P. *Proc Natl Acad Sci USA*. 1996;93(12):6085–6090.
- [85] Kufel J, Kirsebom LA. Residues in *Escherichia coli* RNase P RNA important for cleavage site selection and divalent metal ion binding. *J Mol Biol*. 1996;263(5):685–698.
- [86] Behra PRK, Pettersson BMF, Das S, et al. Comparative genomics of *Mycobacterium mucogenicum* and *Mycobacterium neoaurum* clade members emphasizing tRNA and non-coding RNA. *BMC Evol Biol*. 2019;19(1):124.
- [87] Harris ME, Pace NR. Identification of phosphates involved in catalysis by the ribozyme RNase P RNA. *RNA*. 1995;1(2):210–218.
- [88] Hardt W-D, Warnecke JM, Erdmann VA, et al. Rp-phosphorothioate modifications in RNase P RNA that interfere with tRNA binding. *EMBO J*. 1995;14(12):2935–2944.
- [89] Frank DN, Pace NR. In vitro selection for altered divalent metal specificity in the RNase P RNA. *Proc Natl Acad Sci USA*. 1997;94(26):14355–14360.
- [90] Kazantsev AV, Pace NR. Identification by modification-interference of N-7 and ribose 2'OH groups critical for catalysis by bacterial ribonuclease P. *RNA*. 1998;4(8):937–947.
- [91] Christian EL, Kaye NM, Harris ME. Helix P4 is a divalent metal ion binding site in the conserved core of the ribonuclease P ribozyme. *RNA*. 2000;6(4):511–519.

- [92] Christian EL, Kaye NM, Harris ME. Evidence for a polynuclear metal ion binding site in the catalytic domain of ribonuclease P RNA. *EMBO J.* 2002;21(9):2253–2262.
- [93] Christian EL, Smith KMJ, Perera N, et al. The P4 metal binding site in RNase P RNA affects active site metal affinity through substrate positioning. *RNA.* 2006;12(8):1463–1467.
- [94] Kazantsev AV, Krivenko AA, Pace NR. Mapping metal-binding sites in the catalytic domain of bacterial RNase P RNA. *RNA.* 2009;15(2):266–276.
- [95] Cray SM, Kurz JC, Fierke CA. Specific phosphorothioate substitutions probe the active site of *Bacillus subtilis* ribonuclease P. *RNA.* 2002;8(7):933–947.
- [96] Kaye NM, Zahler NH, Christian EL, et al. Conservation of helical structure contributes to functional metal ion interactions in the catalytic domain of ribonuclease P RNA. *J Mol Biol.* 2002;324(3):429–442.
- [97] Chen WY, Pulukkunat DK, Cho IM, et al. Dissecting functional cooperation among protein subunits in archaeal RNase P, a catalytic ribonucleoprotein complex. *Nucl Acids Res.* 2010;38(22):8316–8327.
- [98] Reiter NJ, Osterman AK, Mondragón A. The bacterial ribonuclease P holoenzyme requires specific, conserved residues for efficient catalysis and substrate positioning. *Nucl Acids Res.* 2012;40(20):10384–10393.
- [99] Liu X, Chen Y, Fierke CA. Inner-sphere coordination of divalent metal ion with nucleobase in catalytic RNA. *J Am Chem Soc.* 2017;139(48):17457–17463.
- [100] Lan P, Tan M, Zhang Y, et al. Structural insight into precursor tRNA processing by yeast ribonuclease P. *Science.* 2018;362(6678). DOI:10.1126/science.aat6678.
- [101] Wan F, Wang Q, Tan J, et al. Cryo-electron microscopy structure of an archaeal ribonuclease P holoenzyme. *Nat Commun.* 2019;10(1):2617.
- [102] Wu J, Niu S, Tan M, et al. Cryo-EM structure of the human ribonuclease P holoenzyme. *Cell.* 2018;175(5):1393–1404.
- [103] Lai LB, Vioque A, Kirsebom LA, et al. Unexpected diversity of RNase P, an ancient tRNA processing enzyme: challenges and prospects. *FEBS Lett.* 2010;584(2):287–296.
- [104] Lin H-C, Zhao J, Niland CN, et al. Analysis of the RNA binding specificity landscape of C5 protein reveals structure and sequence preferences that direct RNase P specificity. *Cell Chem Biol.* 2016;23(10):1271–1281.
- [105] Wells JA. Additivity of mutational effects in proteins. *Biochemistry.* 1990;29(37):8509–8517.
- [106] Zhao J, Harris ME. Distributive enzyme binding controlled by local RNA context results in 3' to 5' directional processing of dicistronic tRNA precursors by *Escherichia coli* ribonuclease P. *Nucl Acids Res.* 2019;47(3):1451–1467.
- [107] Svärd SG, Kirsebom LA. Several regions of a tRNA precursor determine the *Escherichia coli* RNase P cleavage site. *J Mol Biol.* 1992;227(4):1019–1031.
- [108] Kirsebom LA, Svärd SG. Identification of a region within M1 RNA of *Escherichia coli* RNase P important for the location of the cleavage site on a wild-type tRNA precursor. *J Mol Biol.* 1993;231(3):594–604.
- [109] Kirsebom LA, Svärd SG. The kinetics and specificity of cleavage by RNase P is mainly dependent on the structure of the amino acid acceptor stem. *Nucl Acids Res.* 1992;20(3):425–432.
- [110] Jovanovic M, Sanchez R, Altman S, et al. Elucidation of structure-function relationships in the protein subunit of bacterial RNase P using a genetic complementation approach. *Nucl Acids Res.* 2002;30(23):5065–5073.
- [111] Sun L, Campbell FE, Zahler NH, et al. Evidence that substrate-specific effects of C5 protein lead to uniformity in binding and catalysis by RNase P. *EMBO J.* 2006;25(17):3998–4007.
- [112] Brännvall M, Kirsebom LA. Manganese ions induce miscleavage in the *Escherichia coli* RNase P RNA-catalyzed reaction. *J Mol Biol.* 1999;292(1):53–63.
- [113] Warnecke JM, Fürste JP, Hardt W-D, et al. Ribonuclease P (RNase P) RNA is converted to a Cd(2+ ⁺)-ribozyme by a single Rp-phosphorothioate modification in the precursor tRNA at the RNase P cleavage site. *Proc Natl Acad Sci USA.* 1996;93(17):8924–8928.
- [114] Chen Y, Li X, Gegenheimer P. Ribonuclease P Catalysis Requires Mg 2+ Coordinated to the pro-R P Oxygen of the Scissile Bond. *Biochemistry.* 1997;36(9):2425–2438.
- [115] Kazakov S, Altman S. Site-specific cleavage by metal ion cofactors and inhibitors of M1 RNA, the catalytic subunit of RNase P from *Escherichia coli*. *Proc Natl Acad Sci USA.* 1991;88(20):9193–9197.
- [116] Perreault JP, Altman S. Pathway of activation by magnesium ions of substrates for the catalytic subunit of RNase P from *Escherichia coli*. *J Mol Biol.* 1993;230(3):750–756.
- [117] Werner C, Krebs B, Keith G, et al. Specific cleavages of pure tRNAs by plumbous ions. *Biochem Biophys Acta.* 1976;432(2):161–175.
- [118] Jack A, Ladner JE, Rhodes D, et al. A crystallographic study of metal-binding to yeast phenylalanine transfer RNA. *J Mol Biol.* 1977;111(3):315–328.
- [119] Behlen LS, Sampson JR, DiRenzo AB, et al. Lead-catalyzed cleavage of yeast tRNAPhe mutants. *Biochemistry.* 1990;29(10):2515–2523.
- [120] Loria A, Pan T. Recognition of the 5 Leader and the Acceptor Stem of a Pre-tRNA Substrate by the Ribozyme from *Bacillus subtilis* RNase P. *Biochemistry.* 1998;37(28):10126–10133.
- [121] Loria A, Pan T. The cleavage step of ribonuclease P catalysis is determined by ribozyme-substrate interactions both distal and proximal to the cleavage site. *Biochemistry.* 1999;38(27):8612–8620.
- [122] Dreher TW. Role of tRNA-like structures in controlling plant virus replication. *Virus Res.* 2009;139(2):217–229.
- [123] Kirsebom LA, Liu F, McClain WH. The discovery of a catalytic RNA within RNase P and its legacy. *J Biol Chem.* 2024;300(6):107318.
- [124] Brillante N, Gößbringer M, Lindenhofer D, et al. Substrate recognition and cleavage-site selection by a single-subunit protein-only RNase P. *Nucl Acids Res.* 2016;44(5):2323–2336.
- [125] Howard MJ, Karasik A, Klemm BP, et al. Differential substrate recognition by isozymes of plant protein-only ribonuclease P. *RNA.* 2016;22(5):782–792.
- [126] Mao G, Chen TH, Srivastava AS, et al. Cleavage of model substrates by *Arabidopsis thaliana* PRORP1 reveals new insights into its substrate requirements. *PLOS ONE.* 2016;11(8):e0160246.